

IMPACT OF IMPELLER BLADE TRIMMING ON THE PERFORMANCE OF
CENTRIFUGAL COMPRESSORS

By

Daniel Swain

A DISSERTATION

Submitted to
Michigan State University
in partial fulfillment of the requirements
for the degree of

Mechanical Engineering - Doctor of Philosophy

2014

ABSTRACT

IMPACT OF IMPELLER BLADE TRIMMING ON THE PERFORMANCE OF CENTRIFUGAL COMPRESSORS

By

Daniel Swain

Centrifugal impeller blade trimming can be used to modify an existing impeller design to meet a new flow or pressure ratio design point. Using flow trimming, the passage area is reduced from inlet to outlet along the entire meridional length of the impeller to reduce the flow coefficient of the impeller while maintaining the pressure ratio of the baseline impeller. Axial trimming is a method of trimming that reduces the blade height at the impeller exit while maintaining the shroud profile of the original impeller in order to reduce the head coefficient of the impeller while maintaining the original flow range.

In this work, computational fluid dynamics was employed to numerically model four impellers of varying geometries, speeds, and performance characteristics in order to understand the performance effects and limits of modifying the impeller geometry by either flow or axial trimming. Flow trimming was found to be capable of reducing the flow coefficient by between 20 and 50% while maintaining the pressure ratio and efficiency of the baseline impeller. The suitability of an impeller for flow trimming was found to correlate strongly with flow incidence angle. Axial trimming could be employed to reduce the pressure ratio to between 9 and 13% of the baseline pressure ratio before choking in the passage reduced the effective flow range. Impeller performance was found to respond differently to axial trimming based on the diffusion ratio of the baseline impeller.

To my family. To Laura, my partner and best supporter. To Jacob and Colin, my favorite boys. I love you all.

ACKNOWLEDGMENTS

First, thanks goes to my advisor, Professor Abraham Engeda, for his support, encouragement, and guidance; and to the members of my PhD committee. I would also like to thank Michael Cave and Solar Turbines for providing the raw geometry and data that helped set the foundation for this work. In addition, I owe a debt of gratitude to my fellow students in the Michigan State University Turbomachinery Lab and to my coworkers at Rolls-Royce - all of whom have been generous with their time and knowledge when I have distracted them from their own pursuits to help me hash out a problem with my research.

I would especially like to express my deepest gratitude to those teachers and professors who went beyond stuffing my head with knowledge and inspired the curiosity and love of science and learning that has brought me to the brink of my proudest achievement. Chief among those is Rob Sload, a gifted teacher and scientist, who sparked a fire twenty years ago that burns to this day. If I contribute anything to science or inspire anyone to follow my path, it will be because Sload once taught me that physics does not suck.

TABLE OF CONTENTS

LIST OF TABLES	vii
LIST OF FIGURES	viii
LIST OF SYMBOLS	xi
Chapter 1 Introduction and Background	1
1.1 History and Application	1
1.2 Construction and Design	4
1.2.1 Construction	4
1.2.2 Design Methods	6
1.2.3 Design Considerations	9
1.2.3.1 Sources of Loss	9
1.2.3.2 Limitations	10
1.2.4 Analysis	11
Chapter 2 Current State of Study	15
2.1 General Design Considerations	15
2.2 Compressor Performance Modification	19
2.3 Importance of Impeller Trimming	20
2.4 Types of Trimming	21
2.4.1 Radial Trimming	22
2.4.2 Axial Trimming	23
2.4.3 Flow Trimming	25
2.5 Theoretical Effects of Trimming	26
Chapter 3 Modeling Methodology	29
3.1 Computational Fluid Dynamic Theory	29
3.1.1 Motivation for CFD	29
3.1.2 Governing Equations	30
3.1.2.1 Turbulence Modeling	31
3.1.2.1.1 Baldwin-Lomax	32
3.1.2.1.2 Spalart-Allmaras	32
3.1.2.1.3 k-epsilon	32
3.1.2.1.4 k-omega	33
3.1.2.1.5 Wall Funcions	33
3.1.3 Boundary Conditions	34

3.1.4	Meshing	35
3.2	Specific Methodology	36
3.2.1	Geometry Modeling	36
3.2.2	Meshing	36
3.2.3	Boundary Conditions and Fluid Domain Properties	38
3.2.4	Solver	39
Chapter 4	Flow Trimming	42
4.1	Impeller Baseline Characteristics	42
4.2	Comparison of CFD Results with Experiments	43
4.3	Trimming Methodology	50
4.4	Flow Trim Results	51
4.5	Analysis	64
Chapter 5	Axial Trimming	67
5.1	Axial Trimming Methodology	67
5.2	Axial Trim Results	68
5.3	Analysis	76
Chapter 6	Conclusions	79
6.1	Summary	79
6.1.1	Flow Trimming	80
6.1.2	Axial Trimming	80
6.2	Applicability to Design	81
6.3	Next Steps	82
BIBLIOGRAPHY	84

LIST OF TABLES

Table 4.1:	Basic Geometry of Baseline Impellers	43
Table 4.2:	Overall Performance for Baseline Impellers	43
Table 4.3:	Percent Difference Between Experimental and Computational Results for Impeller D	47

LIST OF FIGURES

Figure 1.1:	Typical Operating Range of Compressor Types	2
Figure 1.2:	Cordier Line Diagram - specific diameter vs. specific speed	3
Figure 1.3:	Features of a Centrifugal Compressor	5
Figure 1.4:	Velocity Triangle at Impeller Inlet	11
Figure 1.5:	Velocity Triangle at Impeller Exit	12
Figure 1.6:	Graphical Representation of the Jet-Wake Fluid Flow Model	13
Figure 2.1:	Effect of Blade Sweep	17
Figure 2.2:	Ratio of Axial Length to Exit Diameter vs. Flow Coefficient	19
Figure 2.3:	Radial Impeller Trimming	22
Figure 2.4:	Axial Impeller Trimming Profiles	23
Figure 2.5:	Axial Impeller Trimming Profiles Preserving Shroud Profile	24
Figure 2.6:	Impeller Flow Trimming Profiles	25
Figure 3.1:	3D Representation of a Typical Impeller Geometry and Computational Domain	37
Figure 3.2:	Impeller Meridional Profile	38
Figure 3.3:	Typical Computational Mesh	39
Figure 3.4:	View of Mesh at Leading Edge	40
Figure 3.5:	View of Mesh at Tip Region	41
Figure 4.1:	Effect of Mesh Resolution on Pressure Ratio for Impeller D	45

Figure 4.2:	Effect of Mesh Resolution on Isentropic Efficiency for Impeller D . . .	46
Figure 4.3:	Experimental vs. Computational Results for Impeller D	47
Figure 4.4:	Head Coefficient vs. Flow Coefficient for CFD and Experimental Results for Impeller A	48
Figure 4.5:	Efficiency vs. Flow Coefficient for CFD and Experimental Results for Impeller A	49
Figure 4.6:	Pressure Ratio vs. Mass Flow Rate for Flow Trimmed Impeller A . .	52
Figure 4.7:	Pressure Ratio vs. Mass Flow Rate for Flow Trimmed Impeller B . .	52
Figure 4.8:	Pressure Ratio vs. Mass Flow Rate for Flow Trimmed Impeller C . .	53
Figure 4.9:	Pressure Ratio vs. Mass Flow Rate for Flow Trimmed Impeller D . .	53
Figure 4.10:	Isentropic Efficiency vs. Mass Flow Rate for Flow Trimmed Impeller A	54
Figure 4.11:	Isentropic Efficiency vs. Mass Flow Rate for Flow Trimmed Impeller B	55
Figure 4.12:	Isentropic Efficiency vs. Mass Flow Rate for Flow Trimmed Impeller C	55
Figure 4.13:	Isentropic Efficiency vs. Mass Flow Rate for Flow Trimmed Impeller D	56
Figure 4.14:	Head Coefficient vs. Flow Coefficient Ratio for Flow Trimmed Impeller A	57
Figure 4.15:	Head Coefficient vs. Flow Coefficient Ratio for Flow Trimmed Impeller B	58
Figure 4.16:	Head Coefficient vs. Flow Coefficient Ratio for Flow Trimmed Impeller C	58
Figure 4.17:	Head Coefficient vs. Flow Coefficient Ratio for Flow Trimmed Impeller D	59
Figure 4.18:	Isentropic Efficiency vs. Flow Coefficient Ratio for Flow Trimmed Impeller A	60
Figure 4.19:	Isentropic Efficiency vs. Flow Coefficient Ratio for Flow Trimmed Impeller B	61

Figure 4.20: Isentropic Efficiency vs. Flow Coefficient Ratio for Flow Trimmed Impeller C	61
Figure 4.21: Isentropic Efficiency vs. Flow Coefficient Ratio for Flow Trimmed Impeller D	62
Figure 4.22: Circumferentially Averaged Mach Number for Flow Trimmed Impeller D	63
Figure 4.23: Relative Mach Number at Impeller Exit Near Choke for Flow Trimmed Impeller B	64
Figure 4.24: Percent Difference Between Flow Ratio and Area Ratio for Flow Trimmed Impellers	66
Figure 5.1: Head Coefficient vs. Flow Coefficient for Axially Trimmed Impeller A	68
Figure 5.2: Head Coefficient vs. Flow Coefficient for Axially Trimmed Impeller B	69
Figure 5.3: Head Coefficient vs. Flow Coefficient for Axially Trimmed Impeller C	69
Figure 5.4: Head Coefficient vs. Flow Coefficient for Axially Trimmed Impeller D	70
Figure 5.5: Total-to-Total Isentropic Efficiency vs. Flow Coefficient for Axially Trimmed Impeller A	72
Figure 5.6: Total-to-Total Isentropic Efficiency vs. Flow Coefficient for Axially Trimmed Impeller B	72
Figure 5.7: Total-to-Total Isentropic Efficiency vs. Flow Coefficient for Axially Trimmed Impeller C	73
Figure 5.8: Total-to-Total Isentropic Efficiency vs. Flow Coefficient for Axially Trimmed Impeller D	73
Figure 5.9: Exit Flow angle vs. Flow Coefficient for Axially-Trimmed Impeller D	74
Figure 5.10: Relative Mach Number at Impeller Exit Near Choke for Axially-Trimmed Impeller D at 50% Span	76
Figure 5.11: Ratio of Head Coefficient to Design Head Coefficient vs. Trim Percent	78

LIST OF SYMBOLS

a - speed of sound

b - blade height

c - absolute velocity

e - specific energy

h - enthalpy

k - thermal conductivity

m - mass

n_s - specific speed

q - heat energy

r - radius

u - blade speed

A - area

D - diameter

M - Mach number

N - rotational speed

P - pressure

Q - volume flow rate

R_c - compressor pressure ratio

T - torque, temperature

V - velocity

W - relative velocity

Z - compressor axial length dimension

α - absolute flow angle

β - blade angle, relative flow angle

γ - ratio of specific heats

η - efficiency

ν - kinematic viscosity

ρ - density

τ - shear stress

ω - angular velocity

Φ - flow coefficient

Ψ - head coefficient

Ω - rotational speed

Superscripts and Subscripts

h - hub

o - stagnation property

r - radial direction

s - shroud

u - tangential direction

1 - inlet

2 - exit

Chapter 1

Introduction and Background

1.1 History and Application

In his book, Dixon defines a turbomachine as, "a device in which energy is transferred either to, or from, a continuously flowing fluid." [1] The concept of turbomachinery dates back to at least Heron of Alexandria's steam engine from the first century A.D. Centrifugal compressors are used for gas compression and were first developed around the latter part of the 19th century and were used for industrial applications such as mine ventilation or in pneumatic conveyors. Later, centrifugal compressors were used in the first turbojet engines. [2]

The range of application for centrifugal compressors exists between those of positive displacement compressors and axial compressors in terms of pressure ratio and flow rate as shown in Figure 1.1 [3]. The most familiar application for centrifugal compressors is paired with a turbine in an automotive engine turbocharger, but there are many other applications for which a radial compressor is ideally suited. While the centrifugal compressor has been largely replaced by the axial compressor in most modern turbojet applications because axial compressors are generally more efficient than centrifugals, the relative compactness of a centrifugal compressor means it still holds a significant advantage in turboprop and rotary-wing applications where size and weight are of primary concern. The increase in core compression ratio and resultant reduction in corrected flow in response to demand for increased fuel economy means that centrifugal compressors are beginning to find new life in aerospace ap-

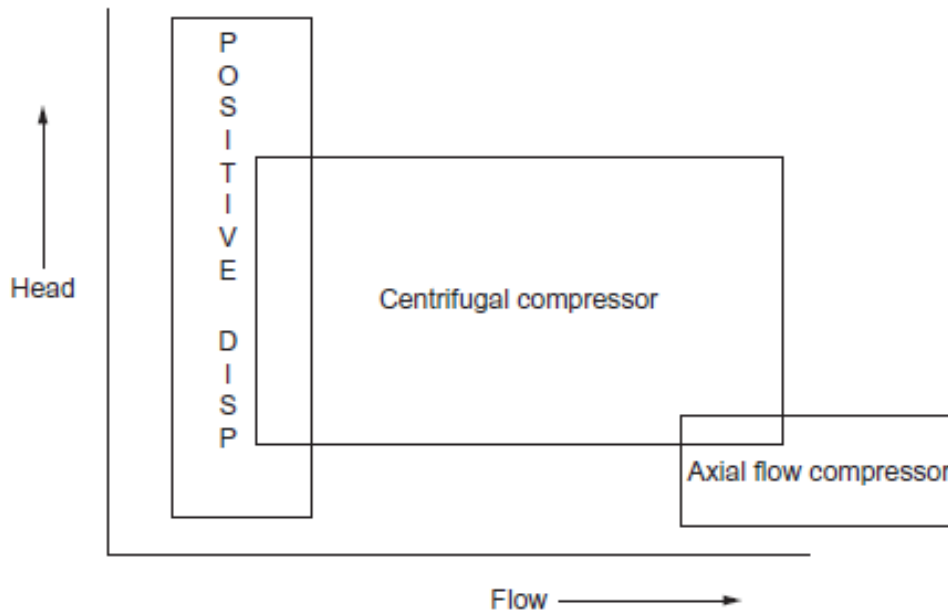


Figure 1.1: Typical Operating Range of Compressor Types

applications as the rear stage of larger turbofan compressors. Centrifugal compressors are also ideally suited for natural gas compression applications because they can produce a much larger pressure ratio over a single stage than an axial compressor and have advantages over positive displacement compressors in that they are able to handle higher flow rates, are more efficient, and have a much simpler mechanical design.

Efficient turbocompressor designs have been found to cluster along a curve first noted by Cordier [4] when specific diameter is plotted against specific speed as seen in Figure 1.2. According to Cordier's work, centrifugal compressors have an advantage over axial compressors below a specific speed of 2.

Of course, reducing the selection of a compressor type to a single parameter is too simplistic, and it is important to consider the advantages and disadvantages of a compressor type relative to other types. For a single stage, a positive displacement compressor can produce a higher pressure ratio than any turbo-compressor, but size increases dramatically

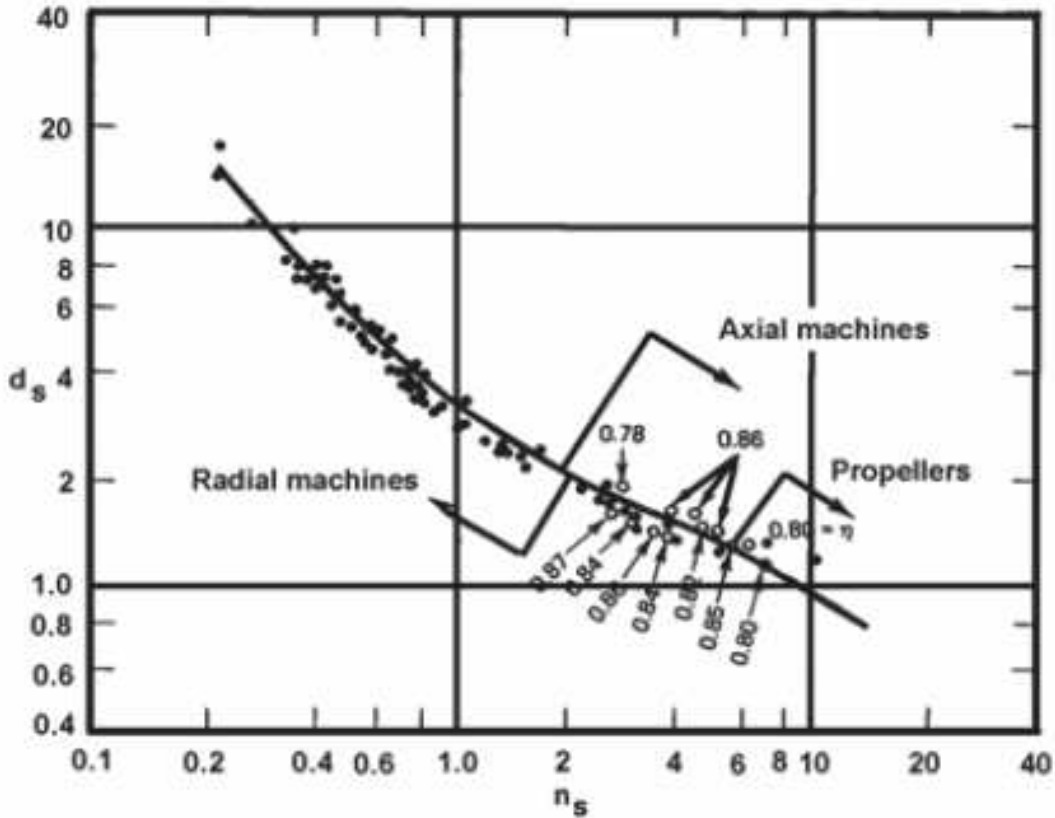


Figure 1.2: Cordier Line Diagram - specific diameter vs. specific speed

with flow rate. Compared with a reciprocating or other positive displacement compressor, a radial compressor has a relative advantage in terms of ability to handle higher flow rates and in mechanical simplicity, as previously mentioned. The disadvantages relative to positive displacement compressors is in the fact that a centrifugal compressor must employ multiple stages to produce comparable pressure ratios and in the fact that a positive displacement compressor produces static pressure while a centrifugal compressor produces both static and velocity pressure which usually must then be converted into static pressure - and so incur losses - in order to be useful. When considering the relative merits of axial and centrifugal compressors, the primary considerations are flow rate and pressure rise. Either axial or centrifugal compressors may be staged to achieve desired pressure ratios and axials hold an

advantage in the fact that the flow may be delivered directly from one stage to the next without the use of elaborate, and loss-inducing, return channels such as those required for staged centrifugal compressors. In addition, an axial compressor can comfortably handle much higher flow rates for a given size than a centrifugal while a radial compressor can generate a greater pressure rise over a single stage than an axial machine. A compromise is sometimes found in a "mixed flow" compressor which exists to fill the gap between centrifugal and axial compressors.

1.2 Construction and Design

1.2.1 Construction

The distinguishing characteristics of a centrifugal compressor are an axial inlet, a 90-degree turn in the flow passage, and a radial outlet. The impeller discharges into a diffuser and then enters a volute or, in the case of a multi-stage compressor, a return channel which turns the fluid into the inlet of the next stage. Figure 1.3 shows the primary features of a typical centrifugal compressor.

Pressure rise in the working fluid is achieved in two ways: the fluid is diffused in the relative reference frame within the passage, raising the static pressure, and additional pressure rise comes through accelerating the fluid in the absolute reference frame and thereby raising the total pressure. This, and the large tangential velocity component of the fluid at the impeller exit, creates the necessity for the diffuser.

A centrifugal compressor diffuser may be vaned or vaneless. Either way, as the fluid travels in the radial direction, the passage area increases and slows the fluid in the relative reference frame converting dynamic pressure to static pressure. Vanes within the diffuser

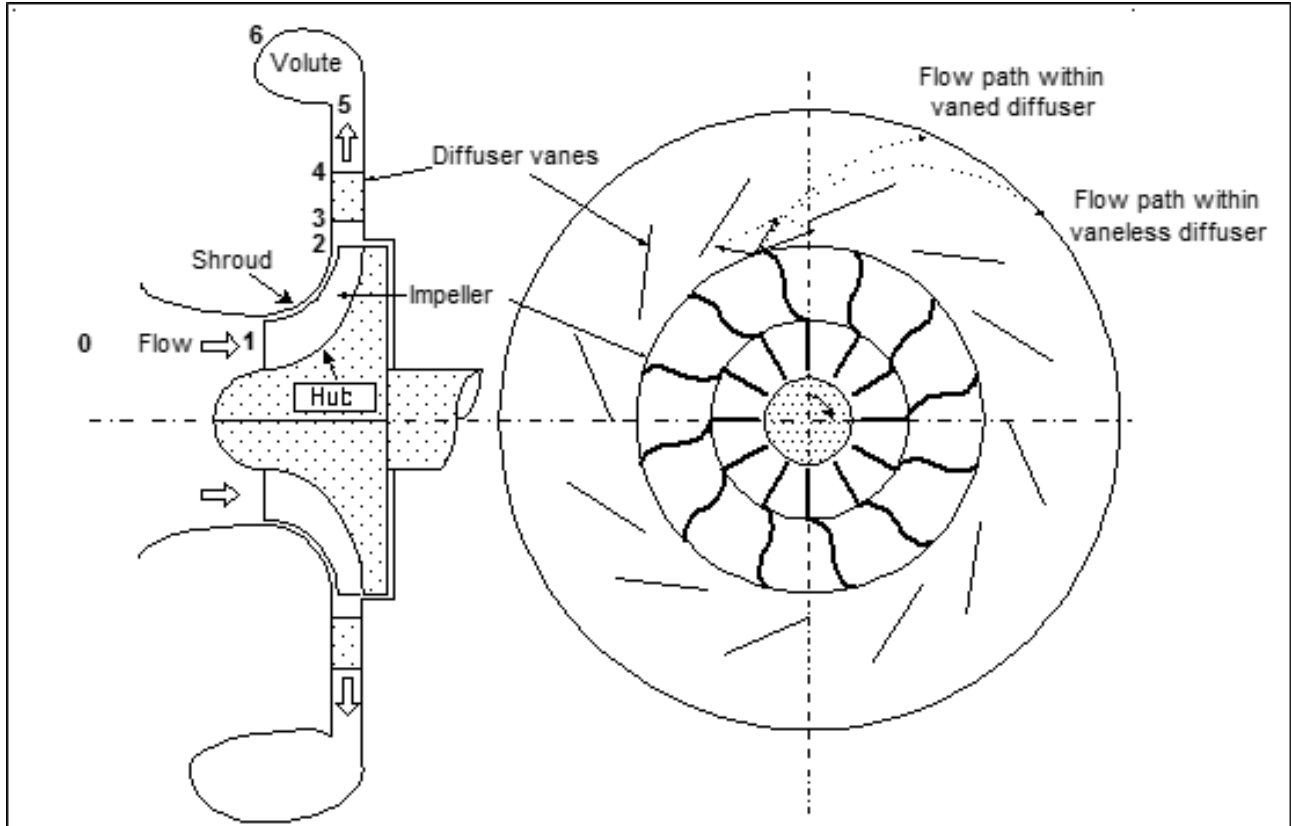


Figure 1.3: Features of a Centrifugal Compressor

may be used to turn the fluid direction from the circumferential to the radial direction. In doing so, the vanes reduce the distance the fluid travels around the diffuser and thereby reduce losses due to diffuser wall friction.

Centrifugal compressors may be constructed using either a shrouded or unshrouded design. An unshrouded impeller has blade passages open on one side that must be matched to a stationary shroud. An unshrouded compressor offers simplicity of construction since the impeller may be machined from a single piece of material, however the unshrouded design means there is a gap between the blade tip and the shroud across which the fluid may leak from the pressure side to the suction side of the blade. A shrouded impeller has the advantage of not suffering from blade tip leakage and is more structurally robust than an

unshrouded impeller, but is more difficult to manufacture since it must typically be made from two pieces of material which must be carefully fit and fastened together. A shrouded design is also more difficult to modify than an unshrouded impeller since the shroud must be removed and replaced in order to trim the blades in the axial direction.

1.2.2 Design Methods

The flow in the channel of a centrifugal compressor impeller is extremely turbulent and complex. High operating speeds - commonly exceeding sonic velocities - and difficulties of visual accessibility make centrifugal compressor flows difficult to analyze. Furthermore, the computing power required to perform numerical CFD analysis has only recently been made available to common users. Historically, centrifugal compressor designs were done empirically and, when a particular design proved successful, was expanded to different applications or operating conditions using laws of similitude. Similitude allows the designer to create a geometrically similar design to a successful design using non-dimensional parameters such as flow coefficient, head coefficient, power coefficient, specific speed, and efficiency. While designs are usually verified or improved using higher-fidelity analysis, similitude laws are often applied to a previous successful design in order to give the designer a reasonable starting point for the new design and so the application of similitude is still common practice in industry. Similitude also gives a set of dimensionless parameters that allows the engineer to quickly evaluate and compare the characteristics of different compressors. Some of the most commonly used parameters are: *flow coefficient* (ϕ), *head coefficient* (ψ), and *specific speed* (n_s). Where:

$$\phi = \frac{4Q}{\pi D_2 U_2}$$

$$\psi = \frac{\Delta P_o}{\rho N^2 D_2^2}$$

$$n_s = \frac{\phi^{0.5}}{\psi^{0.75}}$$

One-dimensional analysis is a useful tool for overall stage design. It helps the designer select major parameters for the impeller design such as inlet and outlet diameters, speed, and inlet and outlet blade angles. However, 1-D design relies on empirically-defined relationships, such as those used for slip or efficiency, to predict compressor performance and does not give the designer any guidance on how to create the blade angle distribution, hub and shroud curvature between inlet and outlet, or how to eliminate losses within the blade passage. Typically, the results of one dimensional analysis are improved by incorporating empirically derived factors to account for slip and sources of loss that do not appear in 1-D equations.

There are many other important parameters related to centrifugal compressor design and performance that affect performance, and describing them all would require turning this work into a textbook, but one that needs highlighting is diffusion ratio. Diffusion ratio is a ratio of the relative fluid velocities at the inlet and exit and is a measure of the amount of diffusion that occurs within the passage. For impellers with a value less than one, there is acceleration rather than diffusion of the fluid within the passage. [5] The equation for Diffusion Ratio is as follows:

$$DiffusionRatio = \frac{W_1}{W_2}$$

Two-dimensional, or meanline, analysis is the application of computational fluid dynamics to the meanline stream surface (measured between hub and tip) of the blade passage of a compressor. 2-D analysis offers more insight into the flow field characteristics than 1-D

analysis with lower computing cost than 3-D CFD, but is obviously limited in its ability to predict performance of the whole flow field since it has no way to directly predict hub or shroud wall friction or tip leakage and cannot account for blade angles that vary between hub and tip. This shortcoming can be partially addressed without excessive penalties in computing cost by using quasi-3D analysis. This is a method by which the flow field is broken into a number of 2-D "slices" along the blade span which allows the flow field to be calculated directly at a number of points along the span and the overall performance to be calculated by interpolating between planes.

Three-dimensional computational fluid dynamic analysis used to be the exclusive domain of high-powered computing, but modern computer technology is now allowing CFD analysis to be performed on desktop computers. There is still significant computational cost to CFD analysis - a typical steady-state solution can take hours or days on a PC and longer for transient analysis. Therefore, 3-D CFD is still too computationally expensive to be used for "white-sheet" design, but multi-core computing brings CFD within the reach of the everyday user. The great advantage of CFD is that a carefully constructed simulation can give a complete flow-field analysis of an impeller and sources of loss such as flow separation can be easily identified, located, and eliminated.

Modern design practice uses a mixture of the tools mentioned. 1-D or 2-D design tools are still useful for initial design and/or parametric analysis. CFD is used to improve and verify the robustness of impeller designs created using similitude or lower-fidelity analysis.

1.2.3 Design Considerations

1.2.3.1 Sources of Loss

As with any compressor, the goal of a successful design is to produce the desired pressure rise at the required flow rate with the least possible work. In order to minimize work input, the losses in the compressor must be minimized, so it is useful to know the sources of loss in a centrifugal compressor.

One of the primary considerations is friction. Friction losses occur on the working fluid within the fluid passage, but also on the back of the disk and in the mechanical components of the compressor. In a shrouded compressor, there is additional loss due to fluid friction on the non-working fluid side of the shroud.

Flow separation can occur within the blade passage on the hub wall, shroud wall, or the blade surface. Fluid separation reduces the effective cross-sectional area of the compressor blade passage in the direction of flow and thereby reduces the diffusion pressure rise.

Blade tip leakage is another source of loss in an unshrouded compressor. In order to keep the impeller turning freely and allow space for material distortion due to centrifugal forces and thermal growth, there must be a clearance gap between the impeller blades and the compressor shroud. This gap allows fluid to pass from the pressure side of the blade to the suction side of the blade. Compressor efficiency has been shown to decline with increasing tip clearance by Schumann et al. [6] and by Senoo and Ishida. [7]

Centrifugal compressors typically operate at very high rotational speeds to accelerate the fluid to create the velocity pressure, and because of this high blade speed the working fluid experiences a sudden acceleration in the tangential direction as it enters the blade passage. If the rotational speed and inlet diameter are large enough, and/or the velocity of the fluid

entering the impeller is high enough, there can be a shockwave created at the inlet of the compressor at the leading edge of each of the blades which creates a pressure loss in the fluid as it crosses the shockwave. An inlet may be transonic where only a portion of the inlet (beginning at the outer edge) is affected by shock losses or fully supersonic. A sonic inlet condition may be mitigated by the use of inlet guide vanes to turn the fluid in the direction of rotation, but doing so reduces the tangential acceleration of the fluid within the impeller and therefore reduces the pressure rise in the compressor. Ultimately, a designer must weigh the relative benefits of the pressure rise that can be achieved by high impeller speeds, the size of the inlet required by the flow rate, and the losses incurred by shock at the inlet.

1.2.3.2 Limitations

In addition to minimizing losses, a centrifugal compressor designer must consider certain limitations of compressor operation. Choke is an operating condition which limits the through-flow in the blade passage. The relative velocity of flow in the passage is limited by the speed of sound, so the choke limitation is determined by the smallest cross-sectional area of the flow path in the direction of flow. When a compressor is operating in a fully-choked condition, the flow rate cannot be increased by reducing the outlet pressure (also known as back pressure) or by increasing the rotational speed of the impeller.

On the other side of the operating line there exists a pair of limiting conditions known as stall and surge. Both conditions occur when the flow is reduced below a certain level. Surge occurs when the compressor flow rate is reduced by increasing the pressure it has to work against. The result is an unsteady and rapidly varying flow rate that generates noise and creates large cyclical stresses on the compressor components. Stall is a phenomenon wherein the flow becomes separated from the compressor wall or blade surface. Rotating

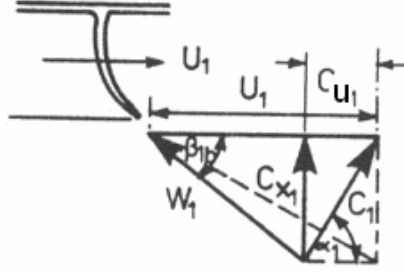


Figure 1.4: Velocity Triangle at Impeller Inlet

stall is a condition in which only a portion of the circumferential area has separated flow. The separated flow regime propagates from blade to blade at a rate on the same order as the rotational speed of the impeller. The repeated and very rapid separation and reattachment of the flow to the blade surface imparts high-frequency cyclical stresses on the blades that can be damaging, especially if the blade has a sympathetic frequency mode.

1.2.4 Analysis

The Euler Turbomachinery Equation as presented in [8] demonstrates how work input creates pressure rise through increasing the tangential velocity of the fluid.

$$T = (\dot{m} + \Delta\dot{m})(c_{u2}r_2 - c_{u1}r_1) + T_F$$

Where $\Delta\dot{m}$ is the fluid leakage and T_F is torque input absorbed by disk friction. The remainder of the torque produces a useful effect by increasing the enthalpy of the fluid.

A basic understanding of the inlet and exit flow can be had by examining the compressor velocity triangles. While simplistic, this analysis provides a great deal of useful insight into the overall performance of the compressor impeller. Figures 1.4 and 1.5 show inlet and exit velocity triangles for a centrifugal compressor.

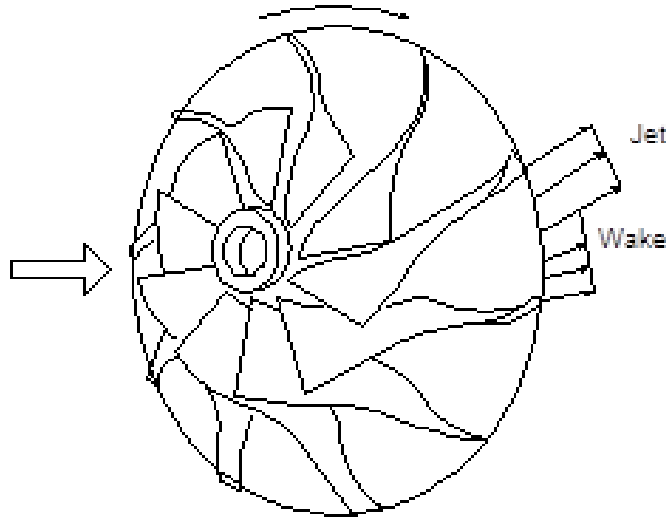


Figure 1.6: Graphical Representation of the Jet-Wake Fluid Flow Model

In this model c_{us} represents the difference between the predicted and actual tangential velocity and β'_2 is the blade exit angle.

The velocity triangle compressor model is useful for understanding the basic inlet and exit flow conditions, but the flow in the impeller is highly non-uniform with large areas of separated flow. A more accurate one-dimensional model is the jet-wake model proposed by Dean [10]. In this model, visualized in Figure 1.6, the fluid exits the impeller with a high-velocity jet near the pressure side of the blade and a large area of low-velocity fluid behind the pressure side of the blade.

The jet-wake model is a useful way to think about the passage flow; however, the flow within the impeller passage is actually far more complex. The low-momentum fluid which comprises the wake is influenced by Coriolis effects, tip leakage flows, and backflow from the diffuser even when the flow field is well-behaved and does not contain large areas of separation. These complex flows can only be modeled using computational fluid dynamics; and, even then, imperfectly.

The efficiency of a centrifugal impeller can reach 95% or better, so it is possible to design an impeller with very low levels of loss, but according to Cumpsty, "The mechanisms of loss generation inside the impeller are not really understood. It is not known, for example, whether the presence of a large wake is really detrimental, nor whether its position affects loss," [11] and so compressor aerodynamic design still relies on the application and modification of previous successful designs. The laws of similitude allow the designer to scale an existing design, but changing the performance of an existing impeller by way of blade trimming is less well understood. The purpose of this study is to explore the effects and limits of impeller performance modification by way of blade trimming. In this way, designers will be afforded an additional tool for centrifugal impeller design or performance modification.

Chapter 2

Current State of Study

2.1 General Design Considerations

In an early study which focused on impellers with straight radial blades, Rodgers found that, "The impeller characteristic is primarily governed by the inducer geometry, in that maximum flow and low efficiency will occur when the inducer chokes, and also as flow is decreased from choke, efficiency will initially rise to a maximum value adjacent to inducer stall and then decrease as a major consequence of inducer stalling losses." [12] Rodgers reports that this is due to the fact that, since the cross-sectional area of the flow passage increases in the streamwise direction, the narrowest portion of the blade passage is found at the inlet, choke will occur at that location. In order to reduce blade blockage at the inlet, some blades are cut back from the inducer portion of the impeller. These partial-length blades, known as "splitter blades" allow the designer to achieve a wider choke margin while maintaining the number of blades necessary to guide the flow at the outlet and limit slip. Also, in low-flow situations, surge phenomena is initiated at the inlet because that is where flow first meets the blades and where separation is initiated.

Because the relative velocity of the leading edge varies in the inducer between the impeller hub and shroud, modern inlet designs employ inlet blade angles that vary in the spanwise direction to maintain an optimum incidence angle along the leading edge. In a 1988 study, Harada found that when a constant inlet blade angle is used, "a large incidence loss at the

inlet occurs as a result of mismatching between the inlet flow and blade angle. In order to achieve a smooth inlet flow into the impeller, and to improve impeller performance, it is necessary to incorporate leading edge twist and to vary blade angles from hub to shroud throughout the impeller.” [13] In that study, it was found that a fully three-dimensional blade angle distribution could improve efficiency as well as increasing both head coefficient and choke flow rate.

As computing tools improve and computing power increases, new studies are able to be designed and executed to improve impeller design. Because there are so many interrelated factors which factor in to turbomachinery designs, they are, ”usually multiobjective problems, where several performance parameters must be considered in the optimization process,” [14] so modern computational methods can be used to automate the design of centrifugal impellers. Bonaiuti and Zangeneh [14] employed a multiobjective genetic algorithm to improve a baseline design to smooth the flow field and thereby improve efficiency across the whole operating range of a compressor as well as extend the choke limit to a higher flow rate.

Many modern impellers are designed with significant backswept blades. This has many beneficial effects such as reduction in blade loading and lengthening of the passage so that more fluid deceleration can occur within the passage rather than in the diffuser - which operates less efficiently. Backswept blades also produce a more radial flow at the impeller exit, and this will tend to decrease the overall pressure rise of the impeller as seen in Figure 2.1. However, because backsweep reduces blade stress, an impeller with backswept blades may be operated at higher speeds, therefore a backswept impeller can achieve a larger pressure rise by the centrifugal effect which is loss-free.

As demand increases for higher pressure ratios and flow capacities, inlet sizes and speeds

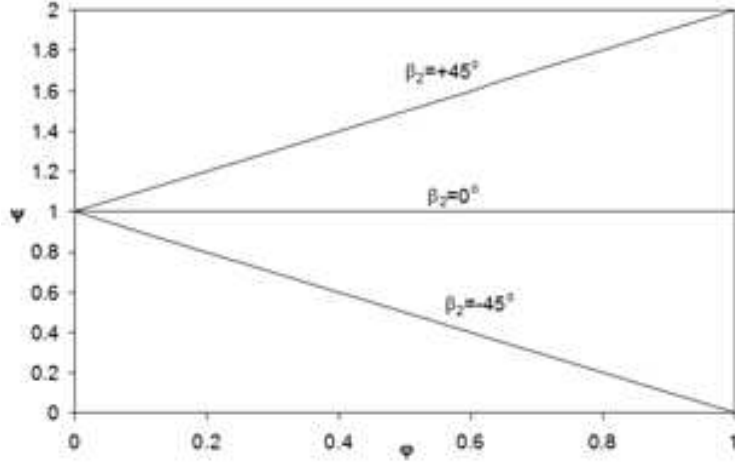


Figure 2.1: Effect of Blade Sweep

increase; and so even well-designed inlets may have shockwaves formed at the leading edge of the blade particularly as the flow rate increases towards choke. There is a pressure loss incurred as the flow crosses a shockwave and so imposes a penalty to the overall pressure ratio of the compressor. Furthermore, in a pair of studies [15, 16] Ibaraki, et al studied the flow field of a transonic impeller and found that an unshrouded compressor suffers an additional penalty. The result of the study found that, in an unshrouded transonic centrifugal compressor, "interaction between the leakage vortex and the shock wave enhances the total pressure loss of the vortex core pitchwise, at downstream of the shock wave."

The clearance distance between the blade tip and shroud of an unshrouded impeller is another key parameter impacting compressor performance. It has been shown clearly by Schumann et al. [6] that increasing tip clearance reduces the pressure ratio of a compressor. That finding was confirmed by Schleer et al. who also found a narrowing of the operating range of a compressor for increased tip clearance because, "for increased tip clearance ratio, stall occurs at higher flow coefficients while the stage pressure ratio was substantially reduced." [17] Intuitively, then, it would seem that decreasing the tip clearance to zero, as

in a shrouded impeller, would improve stall characteristics and increase the operating range, but Harada found that, "A shrouded impeller has inferior overall performance in the lower flow region compared with an identical unshrouded one and also has a narrower stable range, because rotating stall takes place at a higher flow rate." [18]

Another design feature that has attracted some attention from researchers is the axial length of the compressor which can also be described in terms of curvature. As discussed in Section 1.2.1, some portion of the pressure rise in the impeller comes from velocity pressure and some comes from diffusion within the channel. According to Al-Zubaidy, "The so-called 50% reaction design strategy attempts to achieve approximately half the diffusion in the impeller and half in the diffuser. In modern literature the term "diffusion ratio" (which is an indication of static pressure rise) is more widely used." [19] In his mathematical study, Al-Zubaidy proposes that there is a ratio of axial length to outlet diameter (z/D_2) that will produce optimum efficiency. This is due to the fact that a large value for z/D_2 creates a short, wide channel that will cause over-diffusion and flow separation within the channel, but frictional effects become the dominant source of loss as channel length increases. An optimum efficiency band is found to be in the range of about $0.25 < z/D_2 < 0.32$ and the geometry of around 30 impeller designs is found to cluster in that range. In his book, Aungier proposes that the best value for z/D_2 is dependent on flow coefficient and proposes a direct, linear relationship between flow coefficient and z/D_2 as seen in Figure 2.2. [20] These proposals were tested by Sorokes et al. in a computational fluid dynamic study of the effect of shroud curvature (as a proxy for axial length) on impeller performance. A baseline design was modeled through z/D_2 values ranging from 0.21 to 0.30 and the best performance was seen at a value of 0.30 for a flow coefficient of 0.12 [21] giving support to the findings of Al-Zubaidy and Aungier.

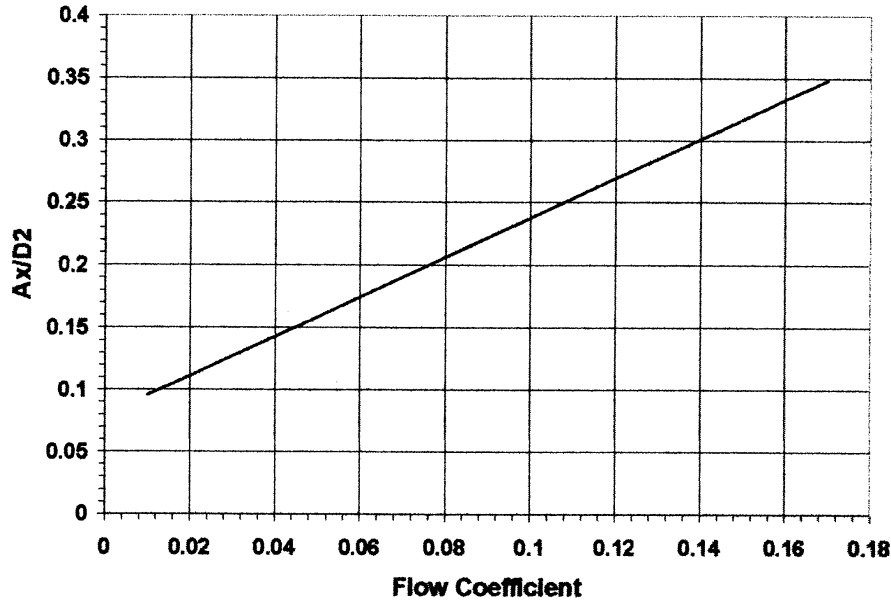


Figure 2.2: Ratio of Axial Length to Exit Diameter vs. Flow Coefficient

2.2 Compressor Performance Modification

It sometimes occurs that the installed operating conditions differ from the design operating conditions, and it becomes necessary to change the performance characteristics of the compressor. However, once installed, the options left to the designer are limited. One of the simplest and most commonly available options is to change the operating speed of the compressor. In this case, the designer needs only to be able to predict the effect of changing the speed of the impeller. A reasonable approximation of the performance change can be made by calculating the difference based on velocity triangles, dimensionless parameters such as ψ , ϕ , and N_s or by using rules of thumb such as those described by Godse: "Head of a compressor varies as the square of tip speed," and "Flow handled by the compressor varies with tip speed and rotor diameter." [22] These methods are useful to a point, but only within a narrow range. If the actual performance goal varies greatly from the original design, then physical modifications must be performed. Furthermore, rotational speed affects both head

and flow, so one cannot be changed by varying rotational speed without affecting the other.

Inlet guide vanes can be used to impart pre-swirl to the working fluid before it reaches the leading edge of the impeller. If the direction of rotation of the fluid is the same as the rotation of the impeller, then the impeller does not accelerate the fluid as much in the tangential direction and so the pressure rise across the impeller is reduced. The opposite is true if guide vanes are used to turn the flow opposite of the impeller rotation. A mathematical model for predicting the effect of changing inlet guide vane angles and comparison with experimental results is presented by Liu et al. [23] The results of the study show that inlet guide vanes are a useful tool for adjusting pressure ratio but that deviating from design conditions comes with a penalty to efficiency.

These methods of performance modification serve a useful purpose in that they are inexpensive and can be applied with relative ease. However, the methods discussed in this section suffer from penalties such as reduced flow range, inability to change head independent of flow, or reduced efficiency. Improved methods of performance modification are available to the designer by physically modifying the impeller.

2.3 Importance of Impeller Trimming

Compressor impeller trimming is a common industrial practice and serves a number of different purposes. In applications where low cost is more important than high efficiency, such as in the production of automotive turbochargers which are manufactured in large quantities and operate using waste energy from the exhaust stream, cast impellers may be machined later in the process to produce impellers with different operating characteristics from a single die. Similarly, a single high-flow design can be expanded to become a family of compressors

by successive trimming in order to cover a wide flow range.

Another important application is the reducing the outlet height of an impeller as described by Lüdtke [8] in order to alter the exit Mach number of an impeller for different molecular weight gases.

In addition to these, it can be very useful to modify an existing impeller design for a new performance requirement rather than perform a "white sheet" design on a new impeller. As discussed previously, modification by the laws of similitude has long been used to adapt successful designs to new operating conditions, but impeller trimming adds additional degrees of flexibility for creating new compressor designs.

Despite these important uses, a lack of research published in open literature has been noted by Rodgers [24] and David [25], and those studies that exist focus on trimming of a single impeller. By examining the effects and exploring the limits of impeller trimming on four different centrifugal compressor impeller designs, this study is an attempt to begin to fill that hole and establish some general guidelines for design engineers who wish to employ impeller trimming as a design tool.

2.4 Types of Trimming

In general terms, there are three primary methods by which a centrifugal impeller may be modified by trimming. The outer diameter may be trimmed, the exit height may be reduced without affecting the inlet, or the blade height may be reduced along the entire passage. These will be discussed individually.

2.4.1 Radial Trimming

In radial trimming, the outlet of the impeller is trimmed in the radial direction reducing D_2 as seen in Figure 2.3. Because the inlet is unaffected, the flow coefficient of the compressor is left unchanged. The purpose of radial trimming is to reduce the total pressure rise across the impeller. This method of trimming can be very useful because it is simple to apply and does not require any modification to the compressor shroud, however reducing the outer diameter does change the exit fluid angle (α_2), and so a vaned diffuser would require redesign. In terms of performance effects, according to Sapiro, radial trimming, "increases the specific speed of the given impeller; therefore, when applied to low specific speed wheels, it displaces their specific speed value closer to the optimum one, while on high specific speed types, it moves them further away into regions of even higher specific speed and lower efficiency."

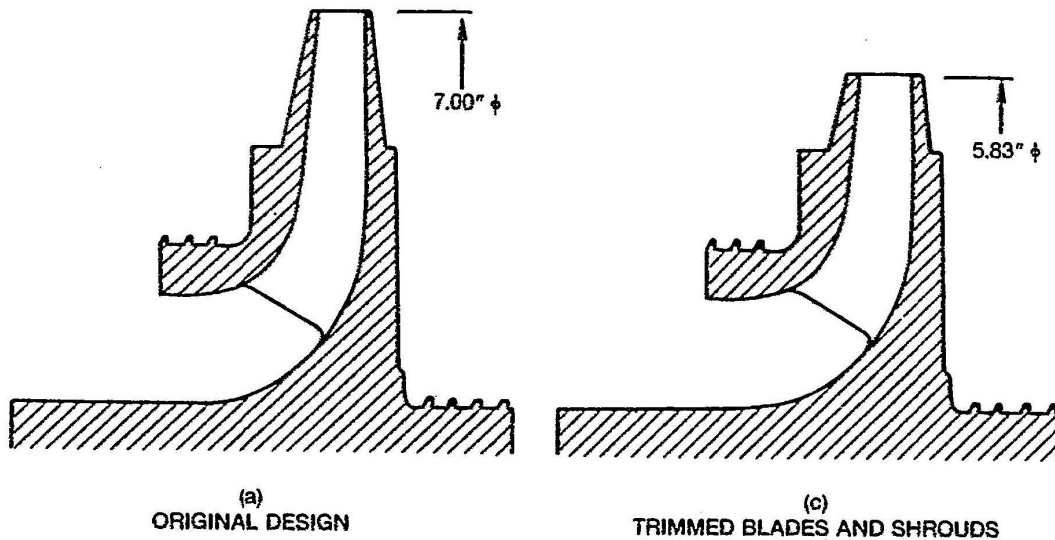


Figure 2.3: Radial Impeller Trimming

This method of trimming does not fundamentally change the flow field in the impeller passage except to shorten it, and so the effects of radial trimming are relatively well-understood and are not addressed in this current work.

2.4.2 Axial Trimming

Axial trimming is a method of trimming by which the impeller blade height is reduced at the outlet of the impeller while leaving the inducer unchanged. This is similar to the method of trimming described by Engeda [27] and Lüdtke [8]. Two representative examples are shown in Figure 2.4.

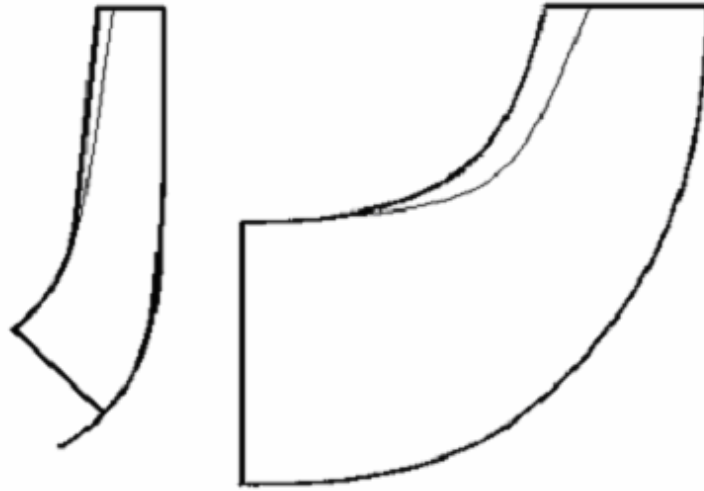


Figure 2.4: Axial Impeller Trimming Profiles

However, in the current study, the outlet blade height is employed to reduce the diffusion in the radial portion of the passage to modify the performance of the impeller rather than to apply an impeller design to a different molecular weight gas. In order to minimize the amount of additional hardware modification, the impeller is trimmed in such a way as to preserve the shroud profile. Figure 2.5 shows a baseline impeller with a series of progressive axial blade trims which preserve the shroud profile shape.

Schumann et al. studied the effects of outlet trimming on a centrifugal impeller. [6, 28] The general trend shown by Schumann is a reduction in the pressure ratio as the outlet of the impeller is progressively trimmed. One significant difference between Schumann's study and the current work is that Schumann maintained the ratio of tip gap to outlet

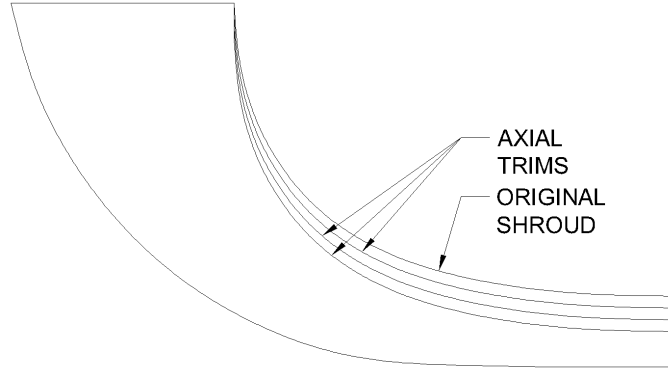


Figure 2.5: Axial Impeller Trimming Profiles Preserving Shroud Profile

blade height so that the tip gap becomes smaller as the blade height is reduced. In doing so, the Schumann study did not isolate the effect of tip gap reduction from the effect of blade trimming. Instead, tip gap losses were reduced as diffusion pressure rise was reduced and channel friction increased. This is a likely explanation for the finding of a local pressure ratio maximum and global efficiency maximum for a progressively-trimmed impeller. A later study by Nili-Ahmadabadi et al. [29] claims to confirm the findings of Schumann’s study, but does not reduce the tip gap in proportion to the outlet blade height, and so the studies cannot be directly related.

In practice, because losses increase with tip gap, the clearance between impeller and shroud is typically reduced to the greatest extent possible and is limited by the impeller exit radius. For a given operating speed, tip gap is largely determined by material distortion which is greatest at the outer diameter, where centrifugal forces have the strongest effect. Therefore, tip gap can usually be considered to be a function of the impeller outlet diameter for a fixed speed and cannot be reduced as the impeller is trimmed. For this reason, and so the effects of blade trimming can be isolated from the effects of tip gap, it is assumed that the blade height of the baseline design has been reduced as far as is practicable for the given r_2 and the clearance is kept constant as the impeller is trimmed.

Axial trimming is proposed as an alternative to radial trimming for high specific speed impellers. Although the modification is more complicated for axial trimming, the limited applicability of radial trimming to high specific speed machines means that axial trimming may have certain relative advantages since reducing the outlet height will lower the specific speed of the impeller and push a high specific speed machine toward a more favorable value of specific speed.

2.4.3 Flow Trimming

The purpose of flow trimming is to modify the flow coefficient of a compressor while leaving the pressure ratio unchanged. Practically, that means reducing the blade height along the entire meridional length of the impeller. A representative meridional view of an impeller blade and a series of flow trims is shown in Figure 2.6.

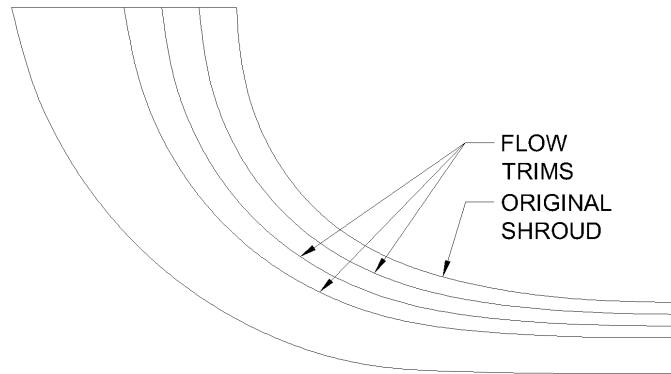


Figure 2.6: Impeller Flow Trimming Profiles

This method of trimming was studied by Rodgers [24] who found a small decline in efficiency for a slightly-trimmed impeller that increases significantly as the impeller is progressively trimmed. In addition, Rodgers' data shows a narrowing of the flow range as the impeller is trimmed. Rodgers also suggests limiting flow trimming to a range of specific speeds between 0.5 and 1.2.

A pair of studies by David et al. [30] and Zhang et al. [25] study the effect of trimming on low specific speed radial compressors. Both studies confirm the findings of Rodgers that flow trimming has a degrading effect on efficiency and flow range. It is also noted that additional losses are due to frictional effects in the flow channel, but Zhang’s study suggests that flow trimming may be useful to specific speeds as low as 0.038 and recommends a limitation of 50% blade height be used as the limit of flow trimming while David’s study does not recommend flow trimming beyond a specific speed of 0.06.

2.5 Theoretical Effects of Trimming

The inlet of a centrifugal impeller is given much more design consideration than the impeller exit. It has already been noted that the impeller inlet is the primary driver of compressor performance. Furthermore, the inlet flow is usually considered to be uniform or, at least, well-behaved; whereas the flow at the exit has thick boundary layers, tip clearance interactions, secondary flows, and a non-uniform exit velocity described in Section 1.2.4. Axial trimming has no effect on the inlet geometry, but flow trimming reduces the inlet area by reducing r_{1s} .

Assuming the inlet velocity is uniform, the mass flow can be found using the equation [1]:

$$\frac{\dot{m}\Omega}{\rho_1 k \pi} = W_{s1}^3 \sin^2 \beta_{s1} \cos \beta_{s1}$$

where $k = 1 - \left(\frac{r_{h1}}{r_{s1}}\right)^2$.

Mass flow is directly proportional to k and k decreases as r_{s1} is reduced. For a 2D blade, β_{1s} is equal to β_{1h} and so does not change as the inlet shroud diameter is reduced. For a 3D blade, where the blade angle changes between the hub and tip β_{1s} will also factor in to

the equation.

Another inlet consideration has to do with losses at the inlet. If the inlet velocity exceeds the speed of sound at the tip, a shockwave will form ahead of the blade and the fluid that crosses it will experience loss. The relative inlet tip Mach number can be found by

$$M_{1s,rel} = \frac{W_{1s}}{a_1}$$

and

$$W_{1s} = \frac{\Omega r_{1s} - c_1 \sin \alpha_1}{\sin \beta_{1s}}$$

According to the above equations, the inlet relative mach number is directly proportional to r_{1s} , so the effect of flow trimming will be to reduce the inlet shock loss of a trans-sonic compressor.

Flow trimming will also have an effect on frictional losses. Because the passage narrows, the ratio of cross sectional area to hydraulic diameter for the passage will decrease and so frictional effects would be expected to have a larger effect on the fluid. Furthermore, since the back plate and rotating mechanical components other than the impeller remain essentially unchanged with flow trimming, the amount of work that goes into raising fluid pressure will decrease while mechanical and disc friction remain unchanged. Therefore, a greater proportion of work input will go to frictional losses, and the compressor efficiency will tend to decrease.

The effects of axial trimming are somewhat more difficult to predict, because outlet height (b_2) is not included in 1-D compressor design. The difficulty arises from the fact that the fluid diffuses within the impeller passage, because the flow within the passage is highly non-uniform. There is, of course flow separation on the suction side of the blade, and the

flow is certainly attached on the pressure side, but it is difficult to predict flow separation on the hub and shroud surfaces or the amount of diffusion that occurs within the passage. If the ratio of static to dynamic pressure rise is known for a given impeller, then some prediction may be able to be made, but there is no generic model for predicting the effect on pressure rise.

Since, as a rule, impellers choke and stall at the inlet, axial trimming should have no effect on the flow range of a compressor in the initial stages. However, trimming narrows the radial passage area, and at some point the choke point will move from the inlet to the knee or radial passage and the choke margin will decrease. In terms of effect of axial trimming on efficiency, any narrowing of the passage would tend to increase frictional effects, and so efficiency would be expected to decrease with axial trimming.

Chapter 3

Modeling Methodology

The study that is the basis of this work was performed primarily using computational fluid dynamics. A series of centrifugal impellers were modeled in CFX [31], a Reynolds-Averaged Navier-Stokes (RANS) flow solver. This chapter will provide some general information on CFD theory and the specific methodology used to model the impellers of interest.

3.1 Computational Fluid Dynamic Theory

3.1.1 Motivation for CFD

Computational fluid dynamics is an important and valuable resource for design and analysis in the turbomachinery industry. The flow field inside a turbomachine is highly turbulent and complex; there is therefore no analytical solution for turbomachinery problems. Engineering correlations are used, and useful, but provide limited information. Experiments usually provide the most reliable data, but one-off hardware is extremely expensive and time-consuming to produce, and therefore not appropriate for iterative design. Furthermore, turbomachines operate at high speeds and are usually optically inaccessible; this places a significant restriction on their usefulness in understanding the properties of the flow field.

Forty years ago, computational fluid dynamics of a sufficient fidelity to resolve the flow field of a turbocompressor was beyond the ability of any computer to perform. Twenty

years ago, CFD could only be performed on mainframe computers; but today a RANS solver can be run on a centrifugal compressor on a desktop computer. This rapid advancement in computing power means that more analysis can be done in less time and the design cycle has been greatly accelerated. For these reasons, most design and a significant amount of analysis of turbocompressors is performed using computational fluid dynamics.

3.1.2 Governing Equations

In CFD, instead of getting an analytical solution for the flow field, the complex fluid domain is discretized into small elements with simple geometry, and the fluid dynamic equations are applied to each one individually. As in any closed system, the laws of conservation of mass, momentum, and energy must apply to every element. The continuity equation for any element is:

$$\frac{\partial \rho}{\partial t} + \frac{\partial(\rho u)}{\partial x} + \frac{\partial(\rho v)}{\partial y} + \frac{\partial(\rho w)}{\partial z} = 0$$

or

$$\nabla \cdot (\rho \vec{V}) + \frac{\partial \rho}{\partial t} = 0$$

In turbomachinery applications, gravitational effects are ignored, so the momentum equations become:

$$\begin{aligned} \rho \frac{Du}{Dt} &= \frac{\partial(\rho u)}{\partial t} + \nabla \cdot (\rho u \vec{V}) = -\frac{\partial p}{\partial x} + \frac{\partial \tau_{xx}}{\partial x} + \frac{\partial \tau_{yx}}{\partial y} + \frac{\partial \tau_{zx}}{\partial z} \\ \rho \frac{Dv}{Dt} &= \frac{\partial(\rho v)}{\partial t} + \nabla \cdot (\rho v \vec{V}) = -\frac{\partial p}{\partial y} + \frac{\partial \tau_{xy}}{\partial x} + \frac{\partial \tau_{yy}}{\partial y} + \frac{\partial \tau_{zy}}{\partial z} \\ \rho \frac{Dw}{Dt} &= \frac{\partial(\rho w)}{\partial t} + \nabla \cdot (\rho w \vec{V}) = -\frac{\partial p}{\partial z} + \frac{\partial \tau_{xz}}{\partial x} + \frac{\partial \tau_{yz}}{\partial y} + \frac{\partial \tau_{zz}}{\partial z} \end{aligned}$$

And, finally, ignoring internal heat generation and gravity, the conservation of energy equation is:

$$\rho \frac{D}{Dt} \left(e + \frac{V^2}{2} \right) = \frac{\partial}{\partial t} \left[\rho \left(e + \frac{V^2}{2} \right) \vec{V} \right] = \frac{\partial}{\partial x} \left(k \frac{\partial T}{\partial x} \right) + \frac{\partial}{\partial y} \left(k \frac{\partial T}{\partial y} \right) + \frac{\partial}{\partial z} \left(k \frac{\partial T}{\partial z} \right) - \frac{\partial(u p)}{\partial x} - \frac{\partial(v p)}{\partial y} - \frac{\partial(w p)}{\partial z} + \frac{\partial(u \tau_{xx})}{\partial x} + \frac{\partial(u \tau_{yx})}{\partial y} + \frac{\partial(u \tau_{zx})}{\partial z} + \frac{\partial(v \tau_{xy})}{\partial x} + \frac{\partial(v \tau_{yy})}{\partial y} + \frac{\partial(v \tau_{zy})}{\partial z} + \frac{\partial(w \tau_{xz})}{\partial x} + \frac{\partial(w \tau_{yz})}{\partial y} + \frac{\partial(w \tau_{zz})}{\partial z}$$

This system of equations comprise the Navier-Stokes equations for three-dimensional, viscous flow. The purpose of the CFD flow solver is to discretize the Navier-Stokes equations. There are many different discretization techniques, and the particular methods are a field of study unto themselves, but the purpose of each is to replace the derivatives with a difference approximation and so convert the partial differential equations into a system of algebraic equations which can be easily solved by a computer.

3.1.2.1 Turbulence Modeling

Turbulence is a major complicating factor in computational fluid dynamics because turbulent flows are irregular, time-dependent, three-dimensional, and essentially chaotic. [32] Turbulence also operates on a wide range of time and length scales. Direct numerical simulation (DNS) of turbulent flows is possible with CFD, but the mesh resolution and time scale must be no larger than a viscously determined scale known as the Kolmogoroff scale. [33] Turbulence also operates on very small time scales so that the computational cost to precisely resolve a turbulent flow field is prohibitive for any but very low Reynolds number flows.

Therefore, when a turbulent flow is modeled using CFD, the overall effects of turbulence are typically approximated by a numerical model. Selecting a turbulence model is an important consideration for CFD and can have a significant impact on the solution.

Large eddy simulation (LES) represents a compromise between accuracy and computational cost by resolving only large scale turbulent flow features and modeling small ones with a numerical approximation; however, for turbomachinery applications, a numerical model is typically used for turbulence at all length scales. A few of the most common models are as follows:

3.1.2.1.1 Baldwin-Lomax The Baldwin-Lomax model is a 0-equation turbulence model that predicts eddy viscosity as a function of the boundary layer velocity profile. Its advantage is low computational cost, but its simplicity also limits its accuracy.

3.1.2.1.2 Spalart-Allmaras The Spalart-Allmaras model [34] is a 1-equation turbulence model that has been used in the gas turbine industry. The Spalart-Allmaras model solves a transport equation for a viscosity-like variable. Like the Baldwin-Lomax model, it has low computational cost, but is less accurate than more sophisticated models.

3.1.2.1.3 k-epsilon The $k - \epsilon$ model is the most commonly used turbulence model for CFD. In it, the effect of turbulence is described as the rate at which kinetic energy of turbulence is converted into heat. The $k - \epsilon$ model is a 2-equation model where k is turbulent kinetic energy and ϵ is the rate of viscous dissipation where:

$$q = k^{1/2}$$

and

$$\epsilon \approx \frac{k^{3/2}}{l}$$

3.1.2.1.4 k-omega The $k - \omega$ turbulence model is another popular 2-equation model similar to the $k - \epsilon$ turbulence model in that turbulent kinetic energy k is one of the variables transported, but differs in that dissipation is determined by a variable, ω , which attempts to model the length scale of the turbulence.

3.1.2.1.5 Wall Functions In flows where the Reynolds number is very high (such as in a turbocompressor), the viscous boundary layer is so thin that it is impractical to refine the grid enough to accurately represent the profile. Therefore, a simplifying assumption about the boundary layer is made by imposing so-called wall functions. Using this assumption, the velocity profile near the wall is modeled by the equation:

$$u^+ = \frac{\bar{v}_t}{u_\tau} = \frac{1}{\kappa} \ln y^+ + B$$

where

$$u_\tau = \sqrt{\frac{\tau_w}{\rho}}$$

where τ_w is the wall shear stress and \bar{v}_t is the mean velocity parallel to the wall, κ is the von Karman constant ($\kappa \approx 0.41$) and B is an empirical constant which is around 5.5 for a smooth flat plate boundary layer. See Section 3.1.4 for a definition of y^+ .

3.1.3 Boundary Conditions

Boundary conditions have a strong influence on the behavior of a CFD solution. Both the value and the type of boundary selected can affect how the model behaves. The primary types of boundary that must be considered are the wall boundary, and the flow inlet and exit boundaries.

In a viscous flow problem, a no-slip boundary is imposed at the wall so that $u = v = w = 0$. Also, since pressure does not transfer across a wall, then $\partial P/\partial y = 0$ for y normal to the wall. However, that is an oversimplification because it ignores viscosity. A more accurate wall boundary condition is:

$$\frac{1}{\rho} \frac{\partial P}{\partial y} = \nu \frac{\partial^2 V}{\partial y^2}$$

Walls in turbomachinery are usually taken to be adiabatic, so where no heat transfers across the wall $\partial T/\partial y = 0$.

The inlet and exit flow boundary types require some a priori knowledge of the flow. For the outlet, a supersonic flow boundary behaves differently than a subsonic flow boundary because the flow across a subsonic boundary can be affected by the boundary condition itself, however information about downstream temperatures, pressures, and velocities do not propagate upstream in a supersonic flow. For an inflow boundary, the opposite is true - if the inlet is super-sonic, then all fluid properties are fixed at the boundary because the upstream flow cannot be affected by the flow field in the computational domain, but only limited information may be transferred into the domain from a sub-sonic boundary. Some assumptions about the flow field such as equilibrium in the direction parallel to the exit plane may be imposed to reduce the distorting effects of a boundary plane, but inevitably the boundary includes some simplifications which will distort the flow field in the region near

the boundary. Therefore, best practice dictates that all boundaries be placed sufficiently far away from the domain of interest that the distorting effects are not experienced by the fluid in the domain being studied.

3.1.4 Meshing

In CFD, the computational grid size and type must be appropriate for the system being modeled. Uniform grids are uncommon in CFD simulations because, in order to capture near-wall flow structures in a meaningful way, they must be refined to the point that the grid imposes a huge computational cost on the model. Unstructured grids are useful when the direction of flow is unknown, but in a turbomachinery application the major structures and directions of the flow are known at least approximately, so structured grids aligned to the direction of flow are typically used.

Because gradients in the flow are usually highest near walls, the grid is typically refined in the near-wall region and spaced more widely away from walls to reduce computational cost. A common metric used to measure grid quality is y^+ value. This is a non-dimensional measure of near-wall grid quality, but can only be calculated after the solution is complete. It is defined as:

$$y^+ = \frac{u_\tau y}{\nu}$$

where y is the distance to the nearest wall.

A smaller value of y^+ corresponds to a finer near-wall grid and is a very useful measure in turbomachinery since velocities in the flow passage are very high and consequently velocity gradients at walls are very high.

3.2 Specific Methodology

All of the compressors in this study were modeled using a four step process: the geometry was modeled, then meshed, the flow solution was generated, and finally the solution is post processed. A detailed description of the process follows.

3.2.1 Geometry Modeling

In each case, a detailed description of the impeller geometry was obtained either from the manufacturer, in the case of Solar Turbines, or from detailed geometry in open literature for the remaining impellers. That geometry was entered into BladeGen software [35]. The detailed geometry included: x,r coordinates for hub and shroud profiles, leading and trailing edge coordinates for both the main blade and the splitter blade (where present), as well as thickness and either beta or theta values at multiple spanwise locations along the meridional length of the impeller blade. The result was an accurate 3D model of the passage geometry. A representative view of the 3D geometry and a meridional profile are presented in Figures 3.1 and 3.2. As noted in Section 3.1.3, the inlet and exit boundaries are located far away from the impeller passage in an effort to minimize the effects of the boundary on the flow field in the region of interest.

The specific geometry of each impeller included in this study is included in Chapter 4.

3.2.2 Meshing

Once the detailed geometry was created in BladeGen, the computational mesh was generated using TurboGrid. [36] A mesh sensitivity study was performed and the results are presented in Chapter 5, but typical computational mesh details are presented here. The mesh is divided

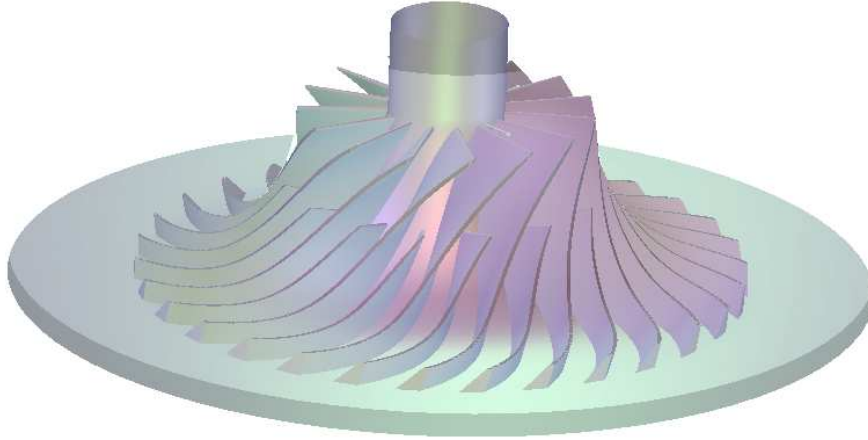


Figure 3.1: 3D Representation of a Typical Impeller Geometry and Computational Domain into three blocks - a stationary block for each of the inlet and exit domain and a rotating block for the impeller. A typical mesh view is shown in Figure 3.3.

Because steady state and axisymmetric behavior was assumed for all cases studied, a sector mesh was used to model the flow field. This is standard practice in the turbomachinery industry and has the advantage of modeling the performance of the compressor with a greatly reduced computational cost. If transient or non-axisymmetric behavior were to arise due to the onset of rotating stall or surge, then the steady-state solution would fail to converge.

The geometry of the inlet and outlet blocks are simple, so a structured hexagonal mesh was used in these regions. In the passage block, an orthogonal mesh was used and refined near the blade surface. A view of the region near the leading edge can be seen in Figure 3.4. Because of flow dependency, it's not possible to set the y^+ value for the mesh precisely, but generally the meshes were kept to a value of around 15 near the blade surface.

The tip clearance region is a zone of very high gradients and so there are 10 elements between the blade tip and the shroud.

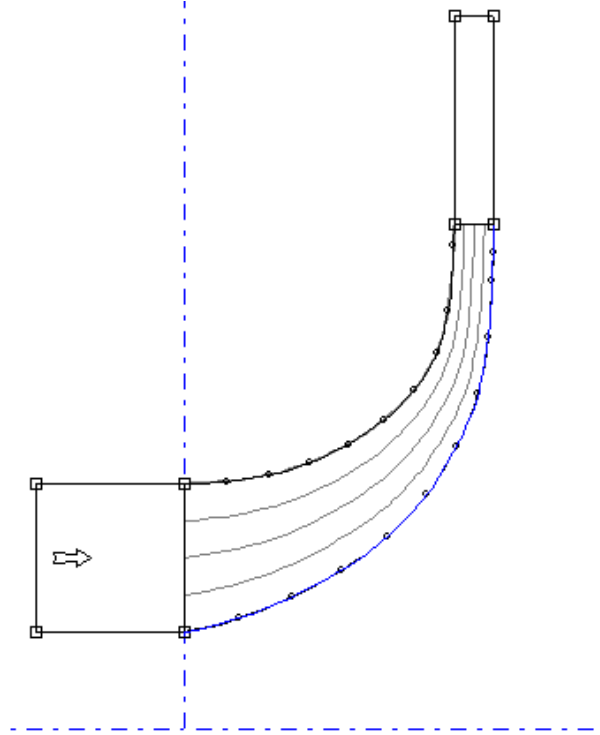


Figure 3.2: Impeller Meridional Profile

3.2.3 Boundary Conditions and Fluid Domain Properties

Setup of the CFD model properties was performed in CFX-Pre which is part of the CFX suite of software from ANSYS [31]. The following applies to each of the impeller models.

The working fluid was air modeled as a non-bouyant ideal gas. The inlet and outlet blocks were stationary with a rotating passage block with a frozen rotor interface between the stationary and rotating blocks.

Walls were modeled as smooth and adiabatic with a non-slip boundary condition. Where an open impeller was modeled, the shroud surface was stationary with a rotating impeller. The fluid at the inlet boundary was subsonic, standard day air (288.2 K, 101.4 kPa) entering with a uniform total pressure and velocity normal to the boundary with medium turbulence intensity. The exit boundary was a subsonic static pressure boundary with the static pressure area-averaged over the whole outlet. The $k-\epsilon$ with wall function model was used to simulate

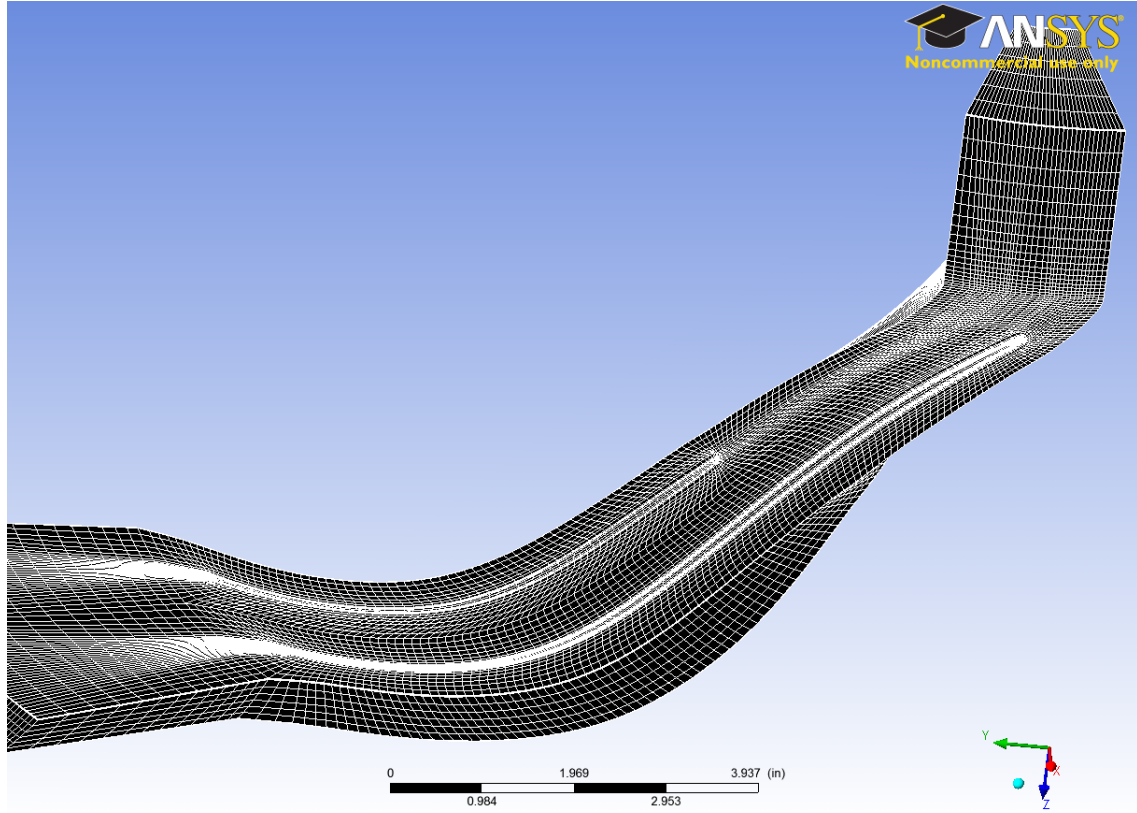


Figure 3.3: Typical Computational Mesh

the effects of turbulence.

3.2.4 Solver

The solver used to compute the flow field was ANSYS CFX [31], a Reynolds-Average Navier-Stokes solver. The high performance compute servers at Michigan State University were used to speed solution convergence. Each computational model was run for a minimum of 1,000 iterations and convergence was considered to be reached when the RMS residuals reached a maximum of 1×10^{-5} and inlet and outlet mass flow differed by less than 0.1%.

Turbocompressors pose a particularly challenging computational problem because, unlike most devices, the flow moves against the pressure field from a region of lower pressure toward a region of higher pressure. Because of this, convergence can be difficult to achieve even for

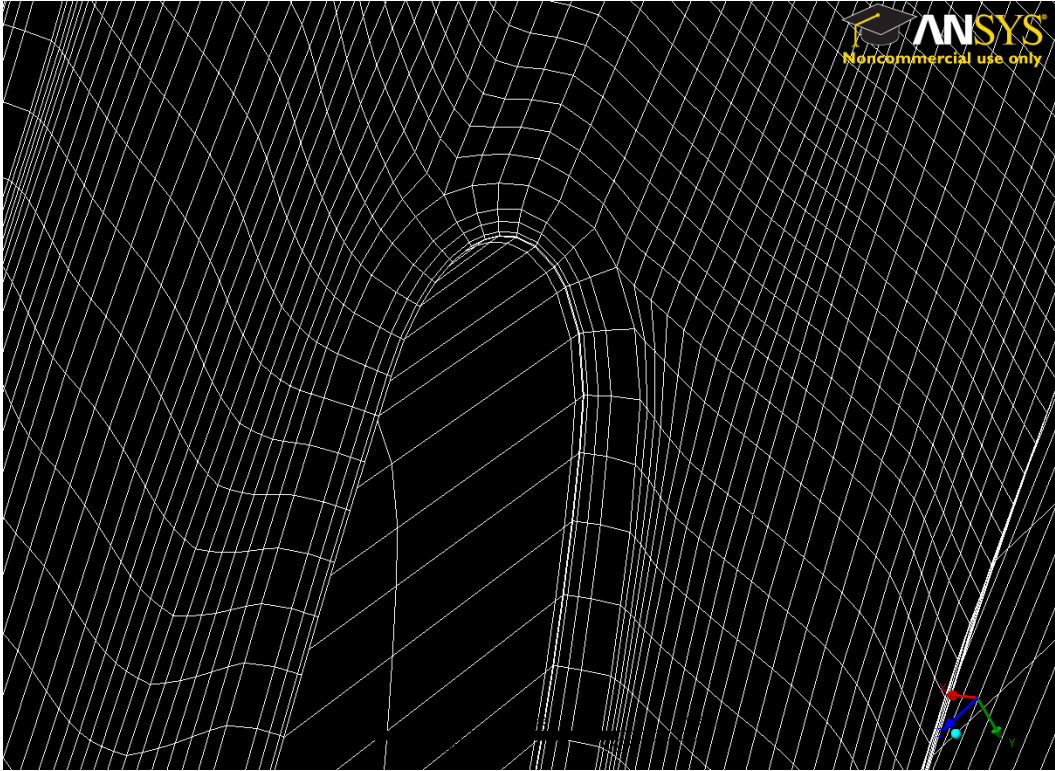


Figure 3.4: View of Mesh at Leading Edge

a steady-state solution. An inappropriate value for a boundary condition will cause non-convergence or reverse flow. A sophisticated CFD code will initialize the flow field in an attempt to improve stability and reduce the time required to reach a converged solution, but even with a well-initialized flow field it can be difficult to achieve solution convergence. A common technique used by designers is to begin with a very low exit pressure so the compressor begins operating in a choked flow condition so the solution has a chance to converge with a lower pressure difference and establish a more accurate flow field. Once a converged solution is realized, the pressure at the exit boundary is raised and the converged solution is used to initialize the flow solution for the new operating point. Too great a change in exit pressure can still cause non-convergence, so this may process may need to be repeated several times, and in doing so, the compressor is 'walked up' the speed line from a choked condition, which is the most stable operating point, to near surge, which is the least stable

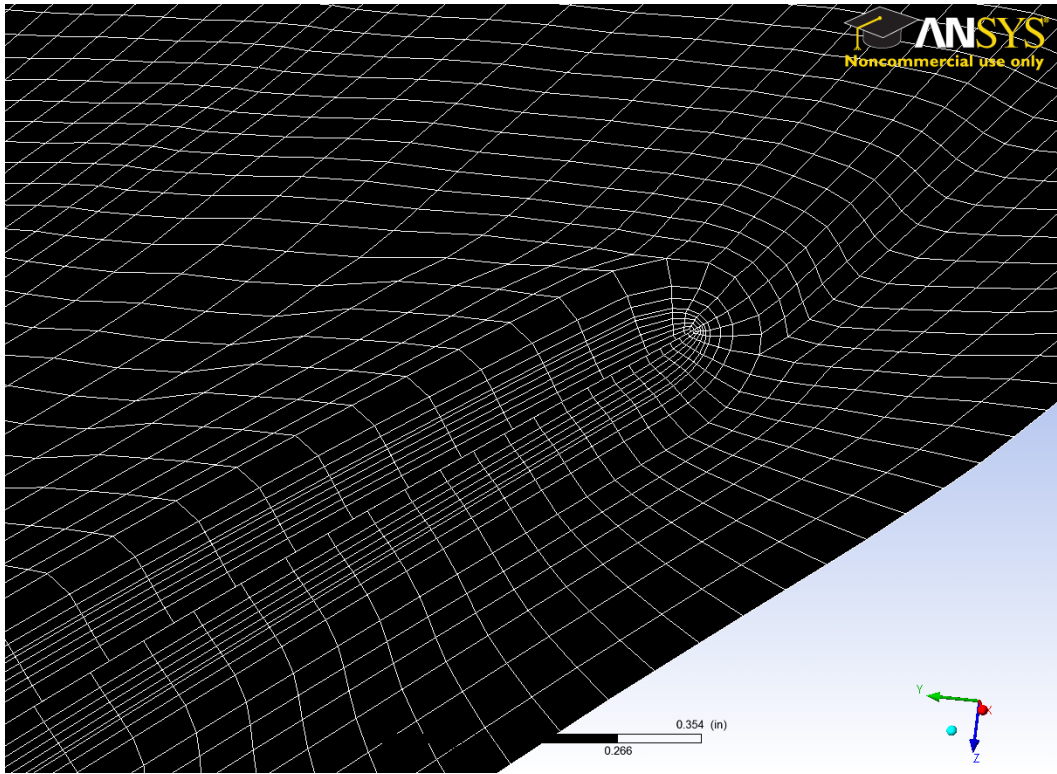


Figure 3.5: View of Mesh at Tip Region

operating point with the highest pressure difference between inlet and outlet. Because surge is an unsteady phenomenon, it can not be modeled using a steady-state CFD model.

Chapter 4

Flow Trimming

4.1 Impeller Baseline Characteristics

For this numerical study, four impeller designs were studied. They were selected because they operated at widely varying conditions. These impellers represent a wide range of nominal performance parameters (pressure ratio and mass flow rate), non-dimensional performance parameters (flow coefficient and pressure coefficient), as well as speed (nominal and specific), inlet Mach number, and so forth. For the sake of simplicity, the four impellers included in this study are labeled Impellers A, B, C, and D and the source of each impeller geometry is as follows:

Impeller A - Solar Turbines proprietary geometry

Impeller B - Coordinates for a High Performance 4:1 Pressure Ratio Centrifugal Compressor [37]

Impeller C - Aerodynamic and Mechanical Design of an 8:1 Pressure Ratio Centrifugal Compressor [38]

Impeller D - The original design geometry is contained in: Splitter-Bladed Centrifugal Compressor Impeller Designed For Automotive Gas Turbine Application [39] with modifications to the geometry as described in Effect of Area Ratio on the Performance of a 5.5:1 Pressure Ratio Centrifugal Impeller [6, 28]

Baseline geometry characteristics for each compressor are presented in Table 4.1 and baseline performance characteristics are presented in Table 4.2.

Impeller	$\omega[rpm]$	$r_{1,h}[cm]$	$r_{1,s}[cm]$	$r_2[cm]$	$b_2[cm]$
A	14000	5.0	11.7	17.8	3.048
B	21789	4.14	10.49	21.56	1.704
C	75000	2.19	4.37	7.98	0.324
D	45337	3.20	5.63	10.15	0.757
Impeller	Tip Gap [cm]	$\beta_{1,h}[deg]$	$\beta_{1,s}[deg]$	$\beta_2[deg]$	No. Blades
A	0.000	40	69	47	9+9
B	0.030	35.8	54.8	49.6	15+15
C	0.025	36.7	56.3	30	19
D	0.174	53.7	62.0	30.2	18+18

Table 4.1: Basic Geometry of Baseline Impellers

Impeller	$\dot{m}[\frac{kg}{s}]$	$P_{o,2}/P_{o,1}$	η_{isen}	Φ	Ψ	N_s
A	3.29	1.54	0.944	0.104	1.11	0.92
B	4.07	4.66	0.928	0.046	1.30	1.96
C	0.86	10.6	0.914	0.056	1.41	0.61
D	0.93	5.68	0.939	0.046	1.56	0.50
Impeller	W_1/W_2	$M_{1,avg}$	$M_{1,s}$	$\beta_{1,b,rms}[deg]$	$\beta_{1,f}[deg]$	Incidence [deg]
A	1.22	0.46	0.55	57.3	56.3	-1.0
B	1.24	0.68	0.82	47.3	53.4	6.1
C	1.49	1.03	1.20	48.1	52.5	4.4
D	1.92	0.76	0.88	58.4	58.1	-0.3

Table 4.2: Overall Performance for Baseline Impellers

In Table 4.2, average values are defined as mass flow averaged, and incidence is defined as the difference between the mass flow averaged relative flow angle ($W_{1,avg}$) and $\beta_{1,rms}$.

4.2 Comparison of CFD Results with Experiments

In order to verify the validity of the CFD results, the numerical models were compared with published experimental results. A full set of experimental data was not available for all the impellers, but the methodology was proven out using experimental data from two impellers

(Impeller A and Impeller D) and applied to the others. The experimental data for Impeller A is proprietary, belonging to Solar Turbines, and is not available in the open literature, but was provided for use in this study. The data for Impeller D is taken from Schumann's study of an axially-trimmed impeller [6, 28].

First, a mesh study was performed at design speed for Impeller D. The mesh was varied from a coarse mesh (50,000 nodes in the impeller passage) to a medium mesh (100,000 nodes) to a fine mesh (250,000 nodes) and the results were compared with the experimental results presented in [28]. For the sake of comparison with experimental results, the CFD model was run to a prescribed mass flow rate at the exit. The results for total pressure ratio vs. mass flow rate are presented in Figure 4.1 and the impeller isentropic efficiency vs. mass flow rate are presented in Figure 4.2. According to these results, the coarse mesh under-predicts the pressure ratio and, more importantly, does not follow experimental trends as the pressure ratio declines at low mass flow rate where the experiment shows a continued increase. Both the medium and fine meshes follow experimental trends well, and both somewhat over-predict pressure ratio, though the medium mesh does not over-predict to the same degree as the model with the fine mesh. In Figure 4.2, it can be seen that all three meshes over-predict efficiency. This is to be expected, because not all the sources of loss experienced by a real compressor are included in the numerical model. These include disk friction on the back side of the impeller as well as mechanical friction due to bearing losses, etc. In industrial practice, this over-prediction in efficiency is commonly accounted for by applying a performance debit to all CFD models. The "medium" mesh was selected for use in the study because using it produced results most consistent with the experimental trends and values.

A full compressor map was run using the "medium" mesh and the design geometry. The

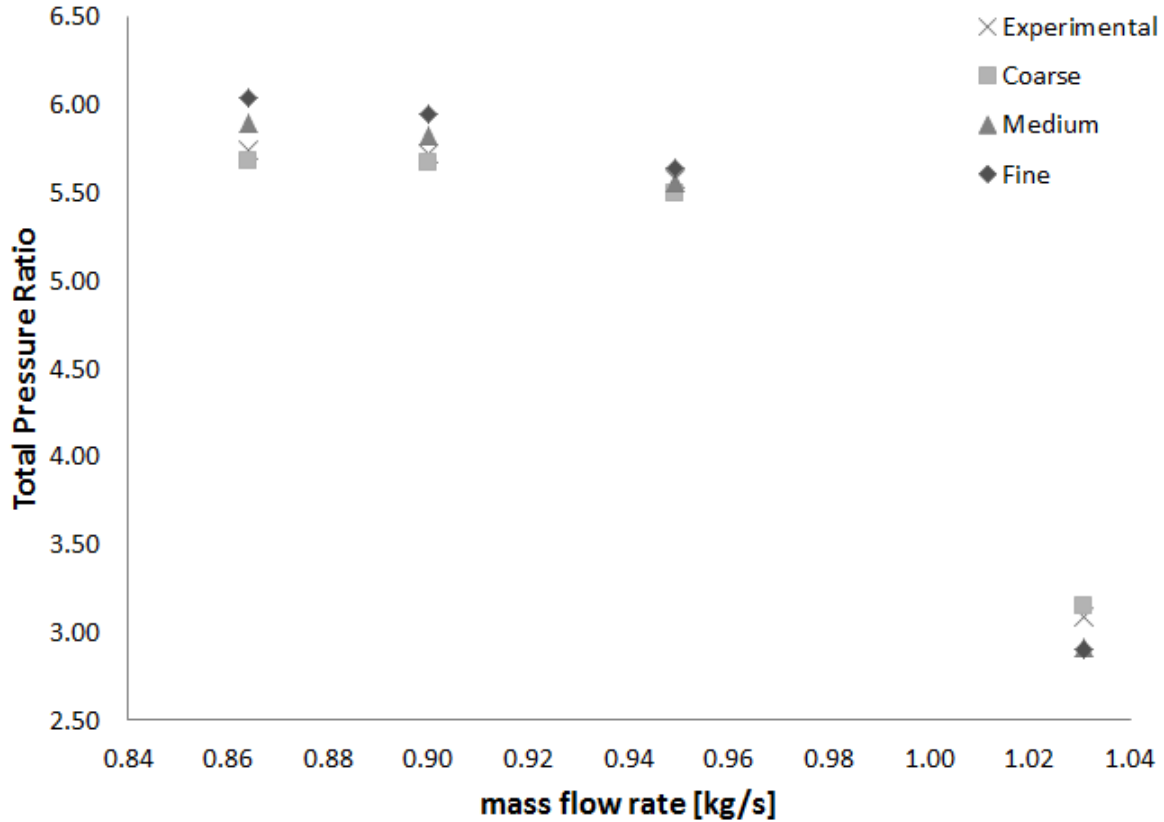


Figure 4.1: Effect of Mesh Resolution on Pressure Ratio for Impeller D

results for pressure ratio and efficiency are presented in Figure 4.3 and in Table 4.3.

Qualitatively, there appears to be a good agreement between all of the experimental data and simulated results. Quantitatively, except for points on the 50% speed line, all predicted pressure ratios are within 2.7% of the experimental values and all efficiencies are within 4.8% of experimentally-measured values.

A full speed line at design speed was also available for Impeller A, as well as a series of flow-trims of that impeller. The results of the numerical model were compared with the experimental data presented in [24]. Figure 4.4 demonstrates good agreement with the experimental data for the baseline and 19.3% trimmed impeller. The more-trimmed impellers follow expected trends, but differ from the experimental data somewhat as head coefficient

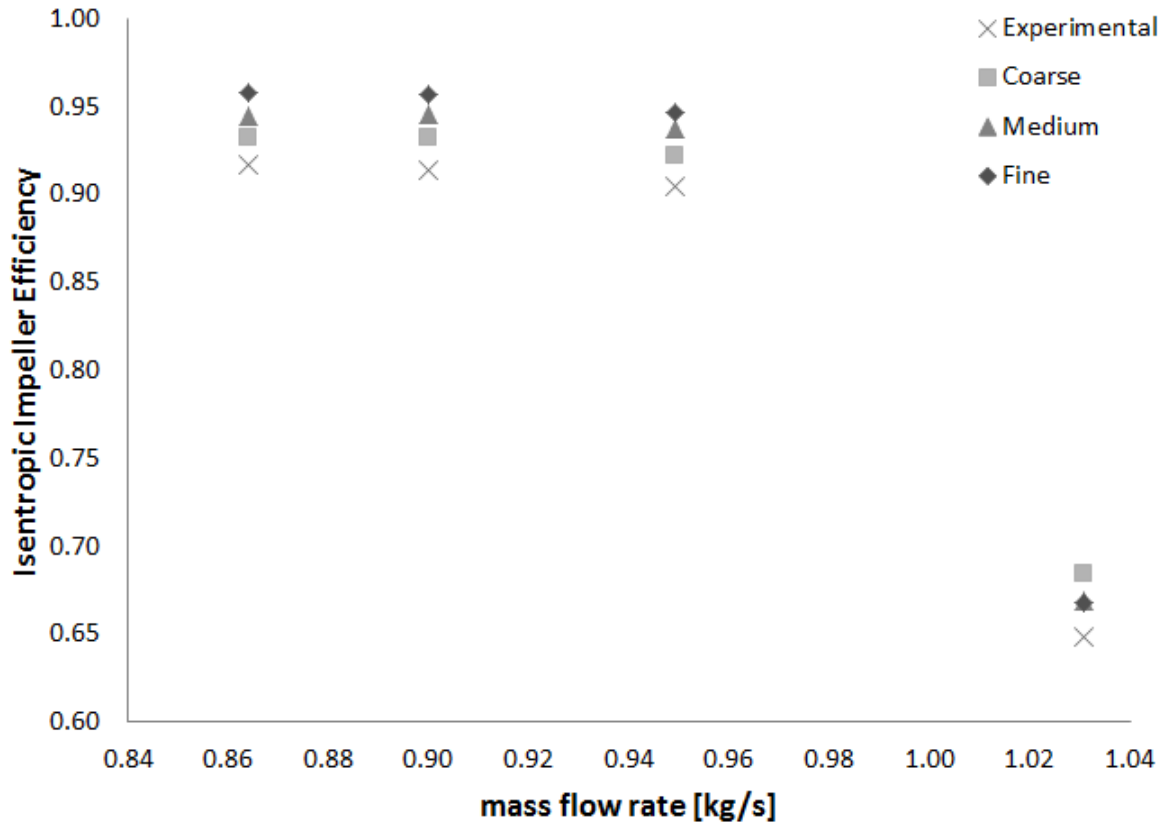


Figure 4.2: Effect of Mesh Resolution on Isentropic Efficiency for Impeller D

risers. This difference can be attributed to the fact that the experiments were conducted using an unshrouded impeller with tight clearances to represent a shrouded compressor. Some tip leakage must necessarily occur when the the shroud is not attached and therefore the difference in head coefficient for the more trimmed impellers is considered to be within the range of expectation. The results for efficiency vs flow coefficient also follow expected trends. Mechanical losses and windage losses on the back side of the impeller are fixed for a given speed; they account for a greater portion of the total power consumed as the impeller is trimmed. Therefore, differences between the numerical and experimental results are expected to be small for the baseline impeller and increase with trimming as demonstrated in Figure 4.5.

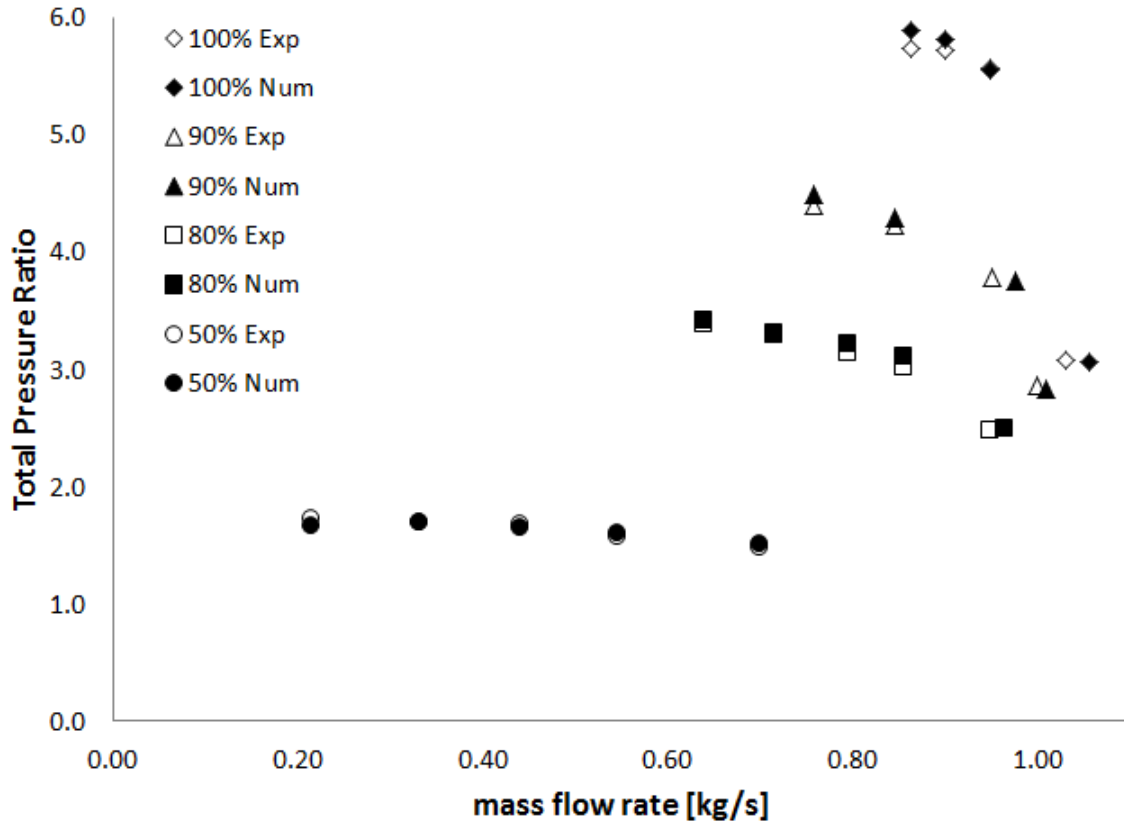


Figure 4.3: Experimental vs. Computational Results for Impeller D

N=45337			N=40803		
m [kg/s]	Rc	η	m [kg/s]	Rc	η
0.864	2.6%	2.9%	0.757	2.1%	3.1%
0.900	1.8%	3.5%	0.846	1.7%	2.7%
0.949	0.3%	3.4%	0.951	2.7%	1.6%
1.058	2.4%	3.2%	1.000	0.9%	4.8%
N=36269			N=27202		
m [kg/s]	Rc	η	m [kg/s]	Rc	η
0.604	1.2%	1.7%	0.214	3.7%	4.1%
0.715	0.6%	1.4%	0.311	0.0%	3.8%
0.795	2.0%	1.9%	0.440	1.0%	1.8%
0.855	3.0%	2.9%	0.546	1.9%	1.6%
0.950	1.6%	2.1%	0.699	2.1%	5.8%

Table 4.3: Percent Difference Between Experimental and Computational Results for Impeller D

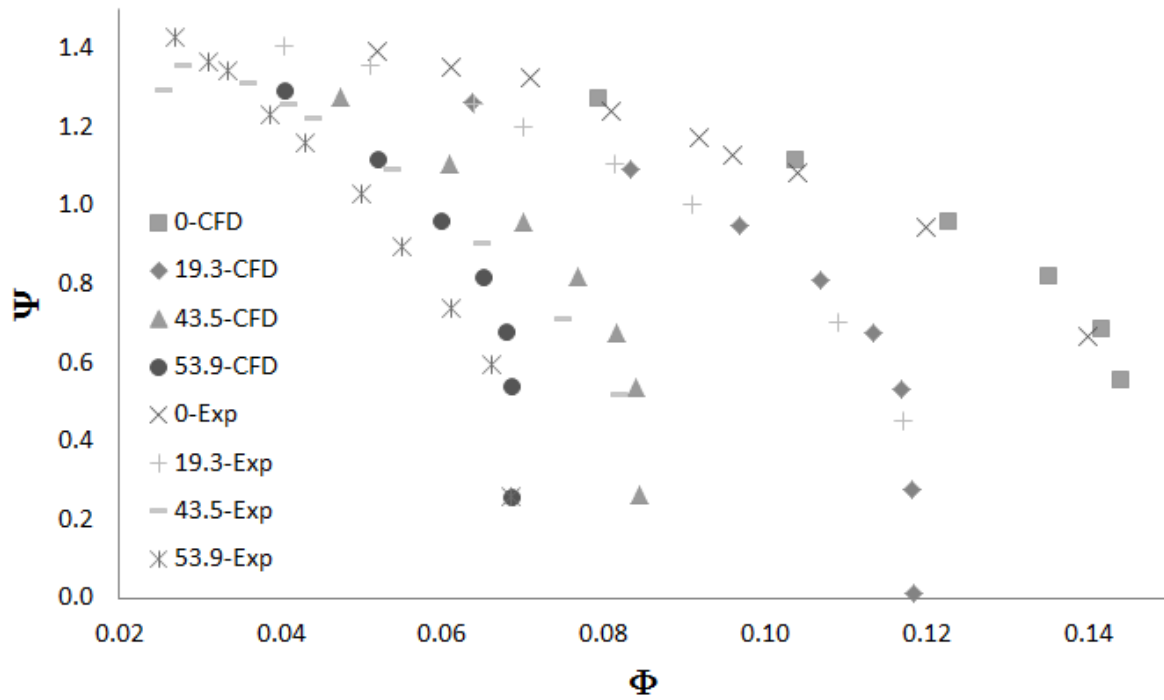


Figure 4.4: Head Coefficient vs. Flow Coefficient for CFD and Experimental Results for Impeller A

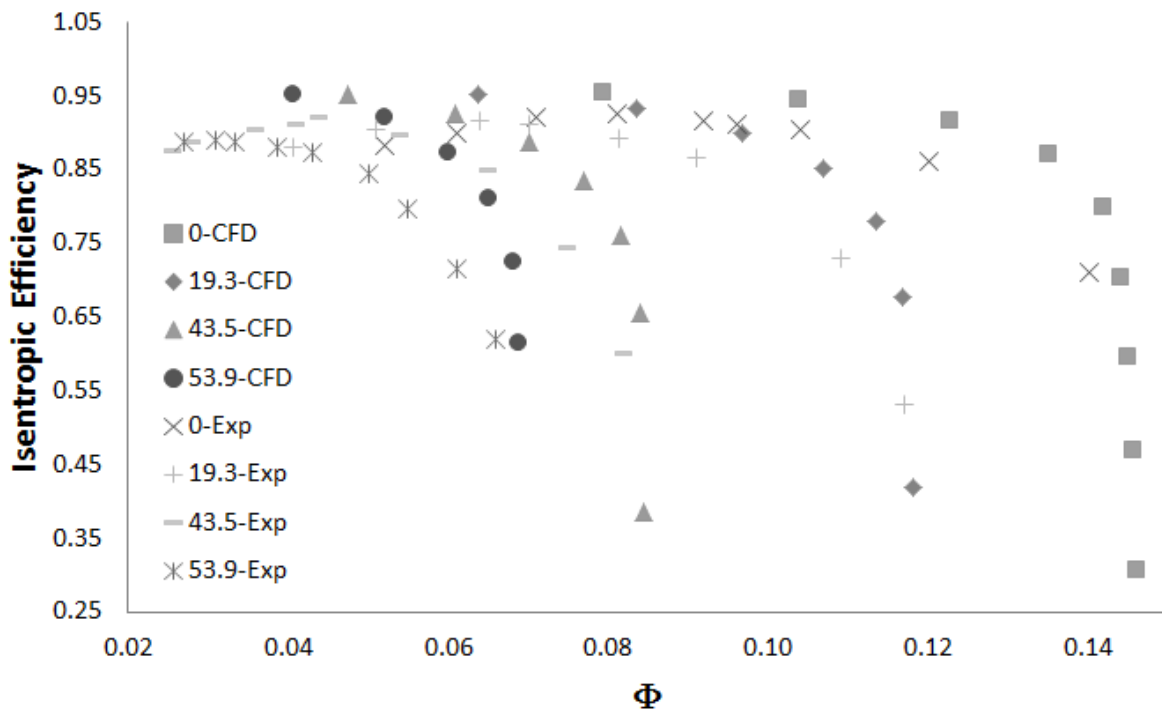


Figure 4.5: Efficiency vs. Flow Coefficient for CFD and Experimental Results for Impeller A

4.3 Trimming Methodology

Because Impeller A was related to established experimental results for a flow trimmed impeller, the trims for that impeller were modeled consistently with the experimental compressor. For the other impellers, the passage was trimmed from inlet to exit according to the following methodology: Both the inlet and exit areas were reduced proportionally so that the ratio of trimmed inlet area to design inlet area is equal to the ratio of trimmed exit area to design exit area.

$$\frac{A_{1,trimmed}}{A_{1,baseline}} = \frac{A_{2,trimmed}}{A_{2,baseline}}$$

The blade is trimmed from the shroud side only, so that the blade height is reduced at inlet and outlet in accordance with the following equations:

$$Area\ Ratio = \frac{A_{1,trimmed}}{A_{1,baseline}} = \pi \frac{r_{1s,trimmed}^2 - r_{1h}^2}{r_{1s,baseline}^2 - r_{1h}^2}$$

and

$$Area\ Ratio = \frac{A_{2,trimmed}}{A_{2,baseline}} = \frac{b_{2,trimmed}}{b_{1,trimmed}}$$

For a particular area ratio, the trim was translated into a percent blade height reduction at inlet and outlet. The spanwise blade height was also calculated at each meridional distance and reduced in proportion to its proximity to the inlet and outlet. In mathematical terms:

$$\frac{Trimmed\ Blade\ Height}{Baseline\ Blade\ Height} = MD \frac{(r_{1s} - r_{1h})_{trimmed}}{(r_{1s} - r_{1h})_{design}} + (1 - MD) \frac{b_{2,trimmed}}{b_{2,design}}$$

where MD is the meridional distance fraction (0 at impeller inlet 1 at outlet).

For each baseline impeller design, a series of trims were applied as described until the inlet area of each impeller was trimmed by at least 60%. Each impeller trim is abbreviated by a letter-number designator where "F" identifies it as a flow trim and the number which follows is the percent area reduction, so an "F30" trim represents a flow trim where the inlet and exit areas have been reduced by 30%. In all cases, the tip gap was kept consistent with the baseline tip gap. In so doing, the effects of trimming are evaluated independent of the effects of varying blade tip clearance.

4.4 Flow Trim Results

Once the geometry for each impeller had been produced, trimmed, and each trim meshed; a speedline was produced for each of the impeller trims. Each model was run from a choked flow condition, and the back-pressure raised to the point that the model failed to converge. The failure of a model to converge at high back-pressure can be assumed to be related to flow instability due to stall or surge, however steady-state CFD has been shown to have limited ability to predict stall in turbomachinery applications [40] [41].

Pressure ratio vs. mass flow for each of the four flow-trimmed impellers is presented in Figures 4.6 through 4.9.

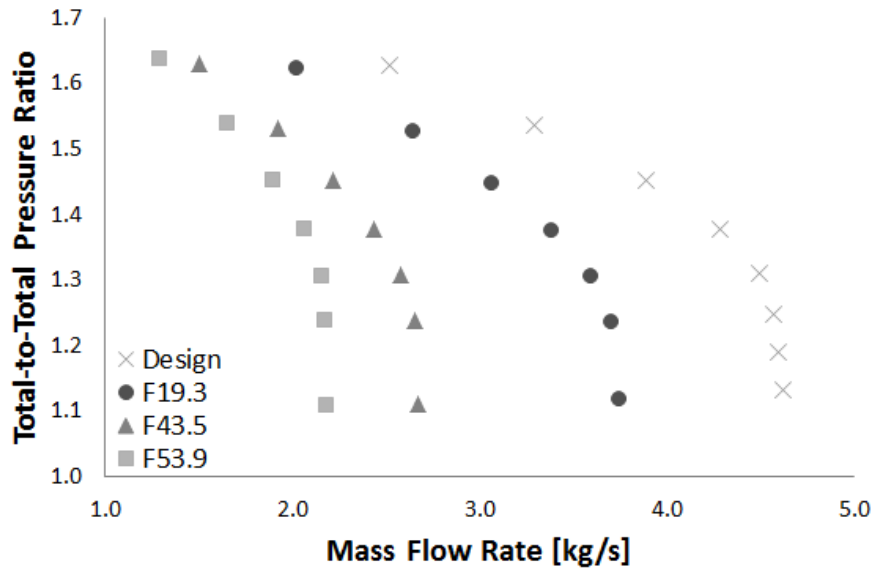


Figure 4.6: Pressure Ratio vs. Mass Flow Rate for Flow Trimmed Impeller A

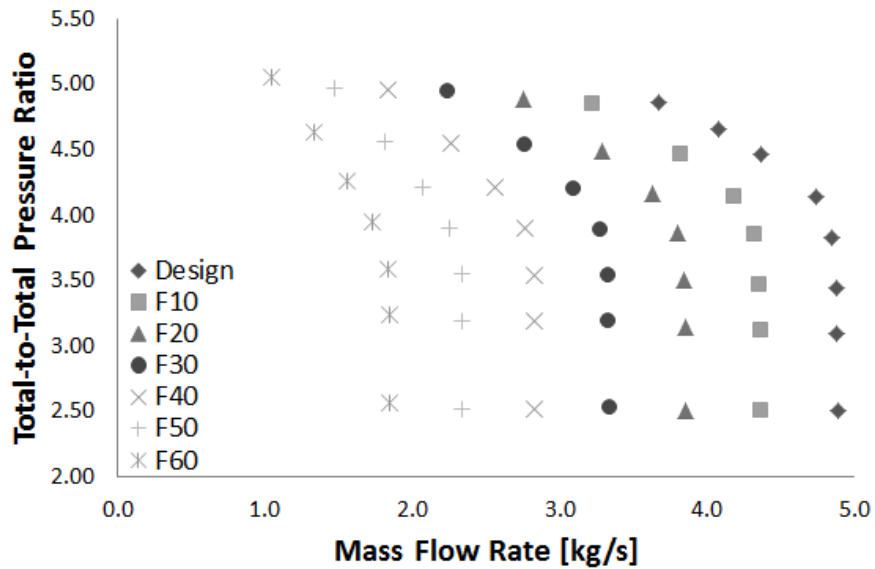


Figure 4.7: Pressure Ratio vs. Mass Flow Rate for Flow Trimmed Impeller B

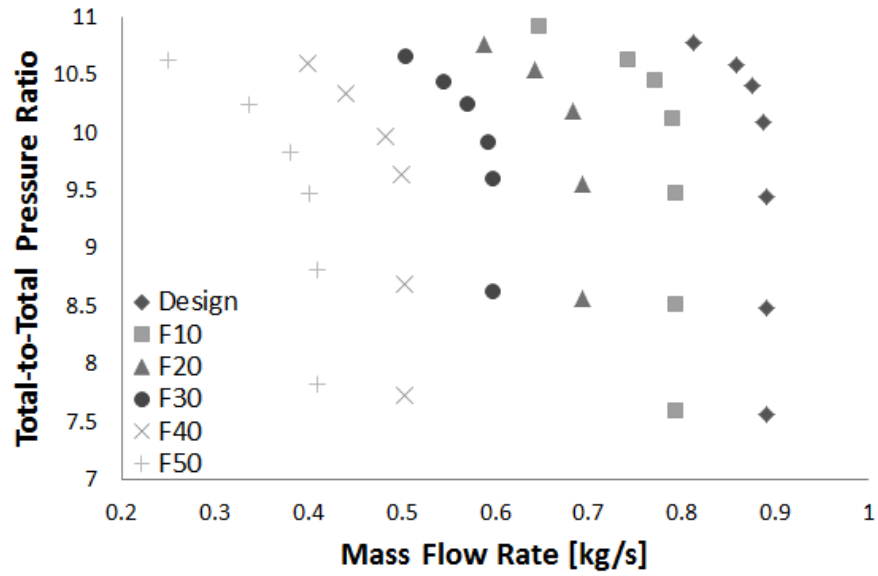


Figure 4.8: Pressure Ratio vs. Mass Flow Rate for Flow Trimmed Impeller C

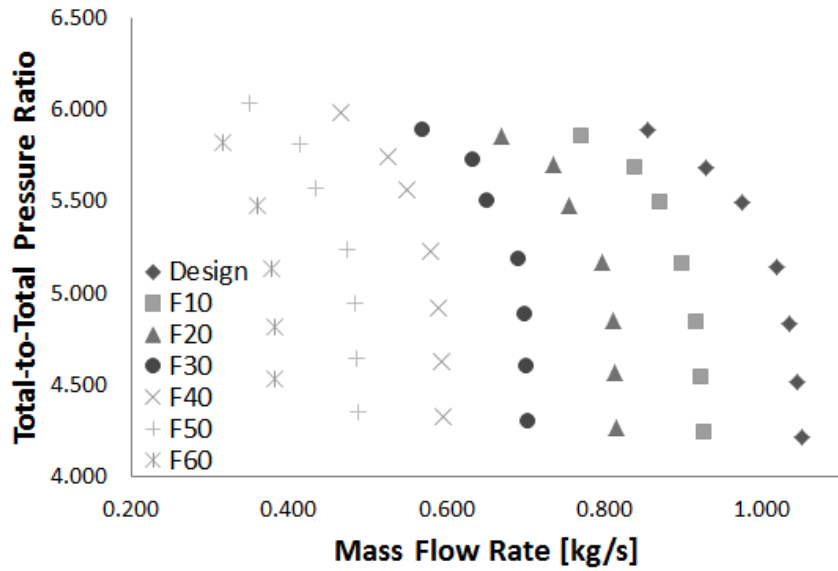


Figure 4.9: Pressure Ratio vs. Mass Flow Rate for Flow Trimmed Impeller D

In each case, it can be seen the choked flow rate is reduced with trimming and the maximum pressure ratio is relatively consistent for all of the impellers except for Impeller C which demonstrates an obvious decline in max pressure ratio as the impeller is trimmed. Most of the impellers (except Impeller C) also show a narrowing of the flow range with progressive trimming. This is in agreement with Rodgers' previous study of flow trimming of Impeller A [24].

Plots of isentropic efficiency vs mass flow rate are shown in Figures 4.10 through 4.13.

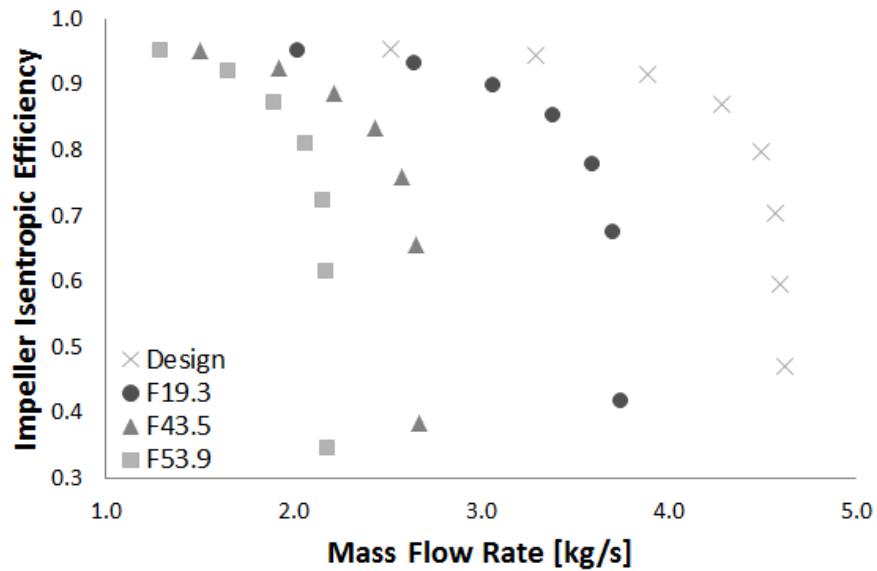


Figure 4.10: Isentropic Efficiency vs. Mass Flow Rate for Flow Trimmed Impeller A

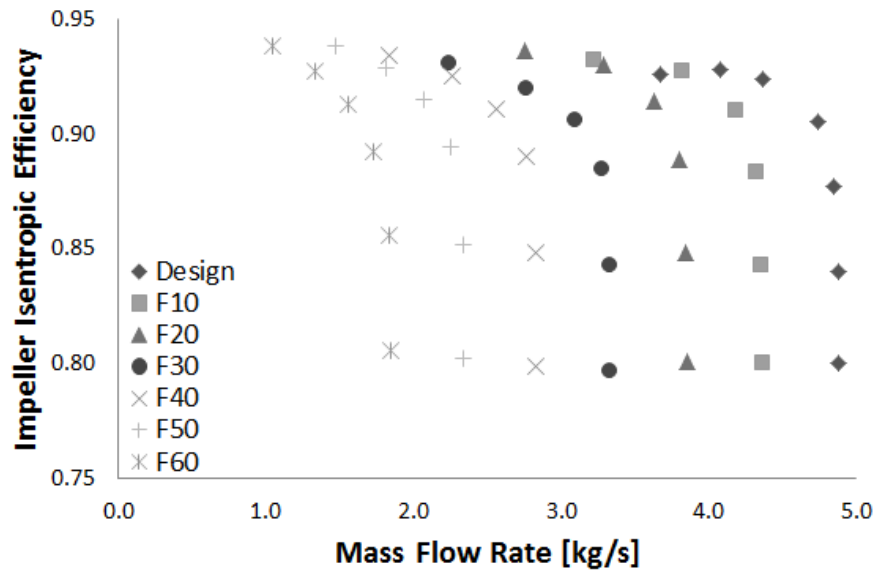


Figure 4.11: Isentropic Efficiency vs. Mass Flow Rate for Flow Trimmed Impeller B

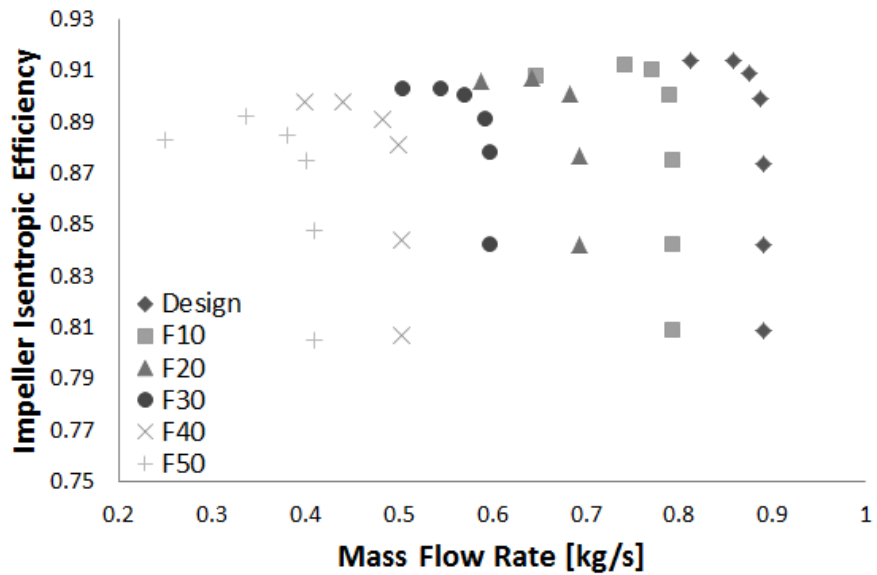


Figure 4.12: Isentropic Efficiency vs. Mass Flow Rate for Flow Trimmed Impeller C

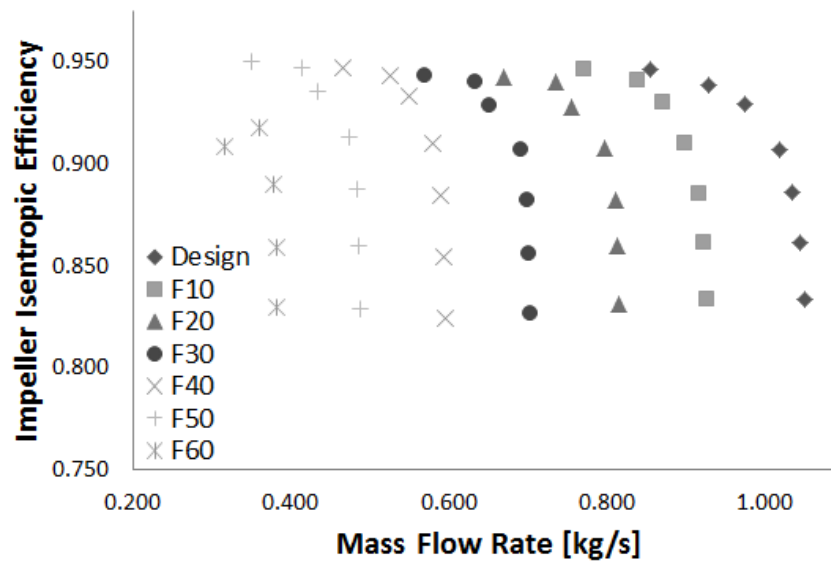


Figure 4.13: Isentropic Efficiency vs. Mass Flow Rate for Flow Trimmed Impeller D

In order to compare the performance of each flow trim, it is useful to nondimensionalize the performance parameters. If the flow coefficient of each trim is divided by the choked flow coefficient then the speed line for a baseline impeller and all trims, then it is much easier to evaluate how the performance of each trimmed impeller compares with the baseline. This ratio will be defined as flow coefficient ratio so that:

$$FlowCoefficientRatio = \frac{\Phi}{\Phi_{max}}$$

Head coefficient is plotted against flow coefficient ratio in Figures 4.14 through 4.17.

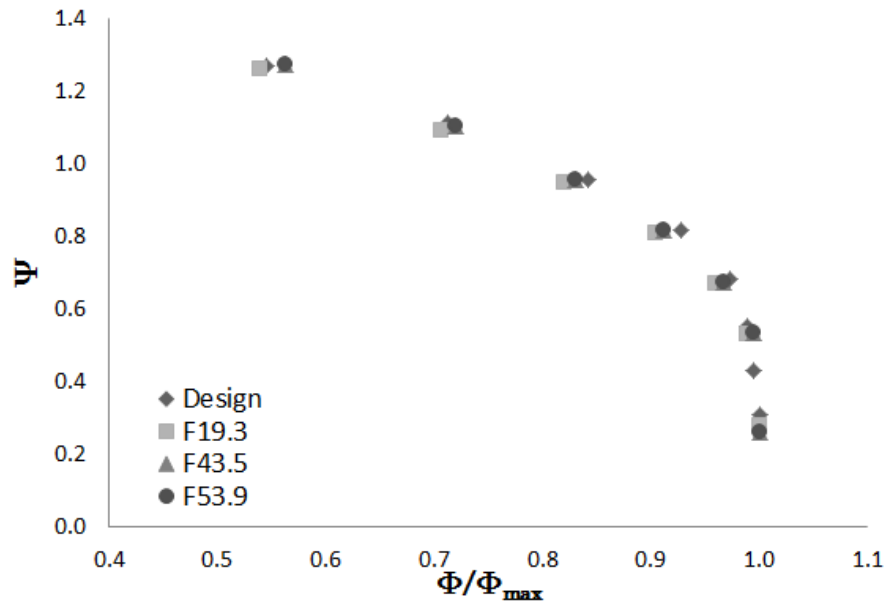


Figure 4.14: Head Coefficient vs. Flow Coefficient Ratio for Flow Trimmed Impeller A

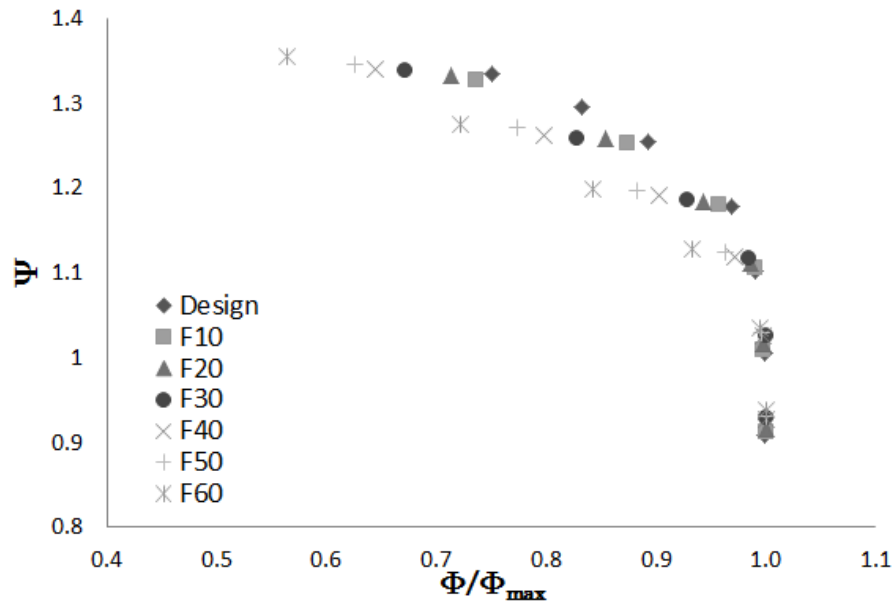


Figure 4.15: Head Coefficient vs. Flow Coefficient Ratio for Flow Trimmed Impeller B

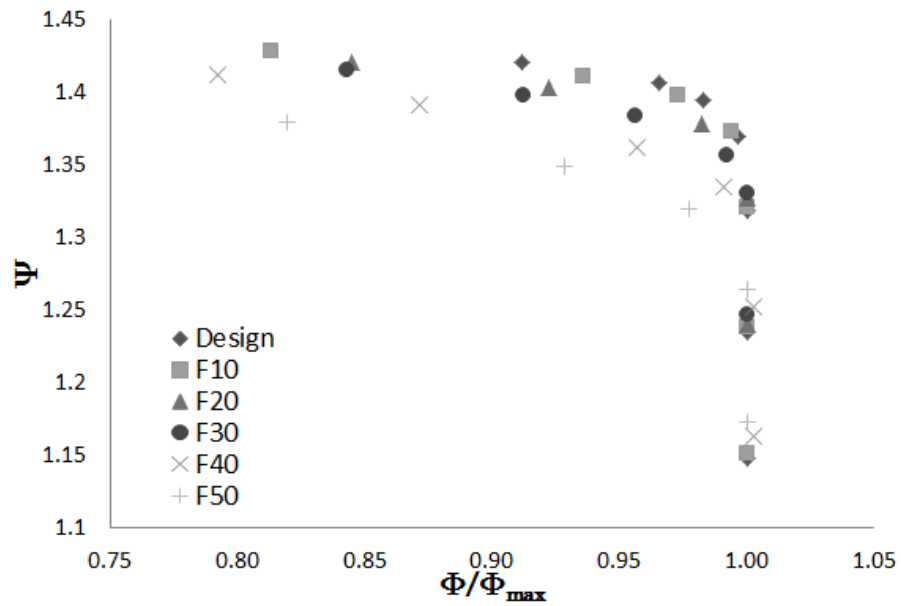


Figure 4.16: Head Coefficient vs. Flow Coefficient Ratio for Flow Trimmed Impeller C

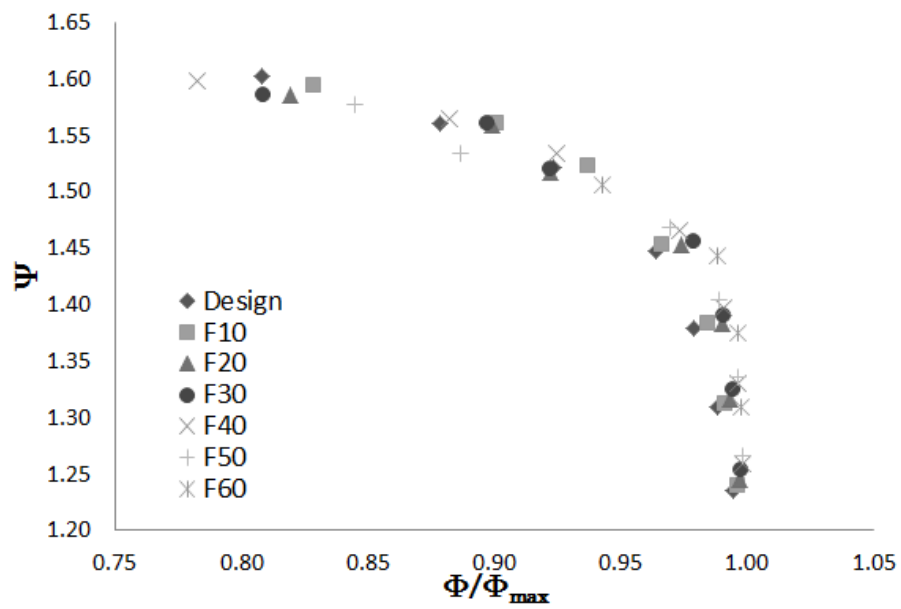


Figure 4.17: Head Coefficient vs. Flow Coefficient Ratio for Flow Trimmed Impeller D

These plots show the head coefficient of Impeller A and Impeller D are insensitive to flow trimming as the flow-normalized speed lines for both impellers are nearly identical to the baseline impeller. In contrast, the head coefficient for Impellers B and C degrades as the impeller is trimmed. In the case of Impeller B, there is a gentle decline in head coefficient as the impeller is trimmed, but Impeller C shows a sudden and significant decline when it is trimmed beyond 30%.

Isentropic efficiency is also plotted against flow coefficient ratio in Figures 4.18 through 4.21.

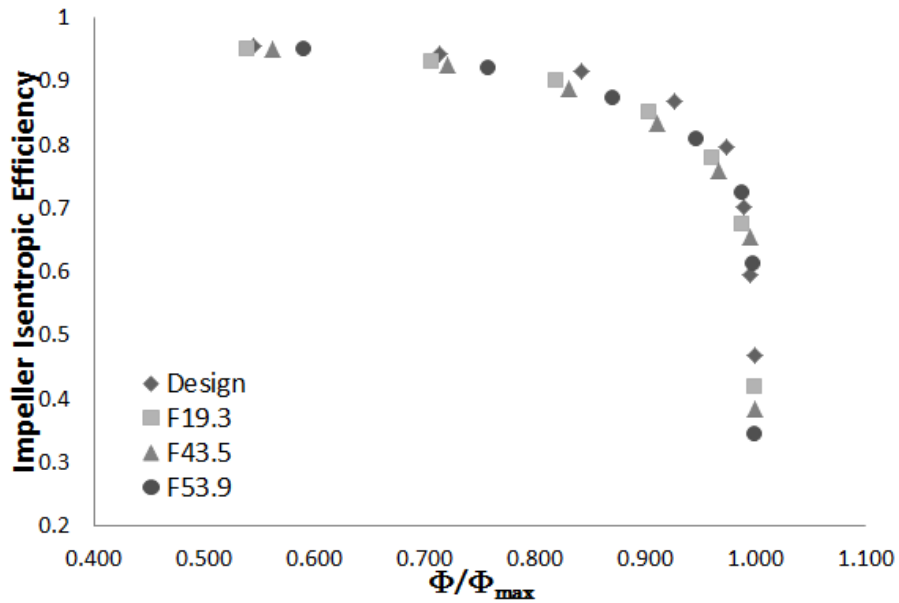


Figure 4.18: Isentropic Efficiency vs. Flow Coefficient Ratio for Flow Trimmed Impeller A

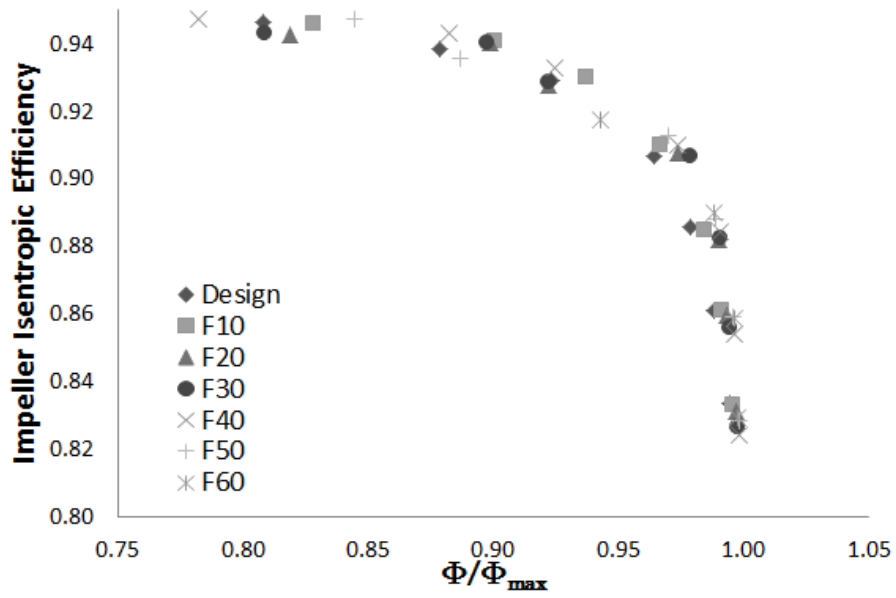


Figure 4.21: Isentropic Efficiency vs. Flow Coefficient Ratio for Flow Trimmed Impeller D

It can be seen that the impeller efficiency reacts very similarly to trimming as the head coefficient. The efficiency of Impellers A and D are relatively insensitive to trimming, but Impellers B and C show significant penalties to efficiency when they are flow trimmed.

An examination of the flow field confirms predictions regarding the effects of flow trimming. Figure 4.22 shows the circumferentially-averaged meridional Mach number profile. The meridional profile does not change much with trimming except in that the inlet tip Mach number reduces with trimming and increases slightly in the passage. This effect can also be seen in the flow field at the exit. Figure 4.23 shows the Mach number profile in the radial portion of the passage. The flow field doesn't change much as the impeller as trimmed except that the Mach number increases slightly and uniformly. This is due to the fact that the ratio of passage area to wetted perimeter reduces as the impeller is trimmed and therefore the boundary layers occupy a larger portion of the passage area. This creates a smaller effective passage area for the fluid to occupy and so the velocity increases. These effects shown in Figures 4.22 and 4.23 are counteractive. Reducing the Mach number at the inlet will tend to decrease loss at the inlet as the impeller is trimmed while increasing velocity in the passage will tend to increase friction losses in the passage.

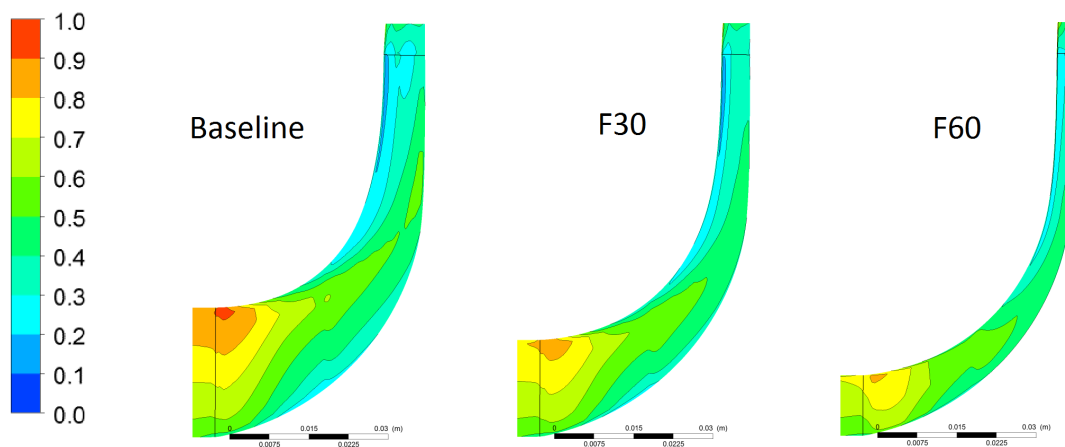


Figure 4.22: Circumferentially Averaged Mach Number for Flow Trimmed Impeller D

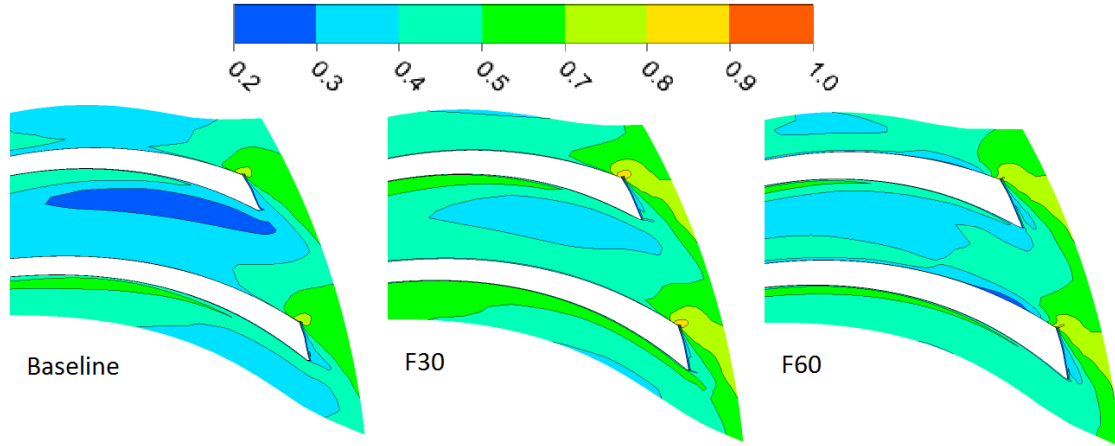


Figure 4.23: Relative Mach Number at Impeller Exit Near Choke for Flow Trimmed Impeller B

4.5 Analysis

The results presented in Section 4.4 demonstrate that an impeller may be trimmed so that the flow coefficient is reduced while the head coefficient is maintained. Furthermore, it is shown that some designs are more tolerant of trimming than others in that the efficiency may be maintained as the impeller is trimmed or there may be a penalty to efficiency with trimming depending on the design of the impeller.

These results confirm Rodgers' [24] finding that trimming narrows the flow range of a compressor, but when the flow is non-dimensionalized by dividing it by the choked flow rate, no reduction in relative flow range is seen. To put it another way, the surge and choke margins do not change for the same Φ/Φ_{max} where surge margin and choke margin are defined as:

$$SurgeMargin = \frac{\Phi - \Phi_{surge}}{\Phi}$$

$$ChokeMargin = \frac{\Phi - \Phi_{choke}}{\Phi}$$

Rodgers also suggests limiting flow trimming to a range of specific speeds between 0.5

and 1.2, however David et al. [30] and Zhang et al. [25] studied flow trimming impellers of much lower specific speed and found that flow trimming could be applied to compressors with specific speeds much lower than the lower bound recommended by Rodgers. This study does not attempt to trim an impeller with such a low specific speed, but confirms those findings in that this study found that a flow trim could usefully be applied to Impeller B, which has a baseline specific speed around 2.0; so no adverse effects were noted when Rodgers' recommended upper limit for application of flow trimming was violated. There may be an upper limit to specific speed for which flow trimming may be applied, but it was not found in this study. Those latter studies also suggest limiting flow trimming to 50% of the original blade height; however, Impeller D could be trimmed as much as 60% of the original blade height while maintaining head coefficient and efficiency similar to the baseline design.

Impellers A and D demonstrated good tolerance for flow trimming in that the efficiency did not decline very much as the impeller was trimmed. Referring back to Table 4.2, the clearest correlation between baseline operating conditions and suitability for trimming exists in the baseline flow incidence where incidence is defined as the difference between the mass averaged inlet flow angle and the blade angle at the RMS inlet radius. Both Impellers B and C have positive incidence, while Impellers A and D have neutral or slightly negative flow incidence.

Because a centrifugal impeller typically chokes at the inducer, the choked flow rate of a flow-trimmed impeller would be expected to scale with the impeller inlet area. In this study, the choked flow rate for a trimmed impeller was found to scale slightly differently than the inlet area. If "Area Ratio" is defined as the ratio of the inlet area of a trimmed impeller to its baseline impeller and "Flow Ratio" is the ratio of the choked flow rate of a trimmed impeller to its baseline impeller, then the percent difference between the two describes how

the flow-trimmed impeller flow rate scales with inlet area. The percent difference between area ratio and flow ratio is plotted against area ratio in Figure 4.24. This graph shows an approximately linear increase in the difference between area ratio and flow ratio as the impeller is trimmed for each of the impellers studied. Impellers B, C, and D all demonstrate similar behavior in that there is an increasing difference between the inlet area ratio and the flow ratio as the impeller is trimmed. Significantly, Impeller A demonstrates much different behavior than the other impellers. This may be due to the fact that Impeller A is the only shrouded impeller studied, but there is insufficient data for shrouded impellers to draw such a conclusion.

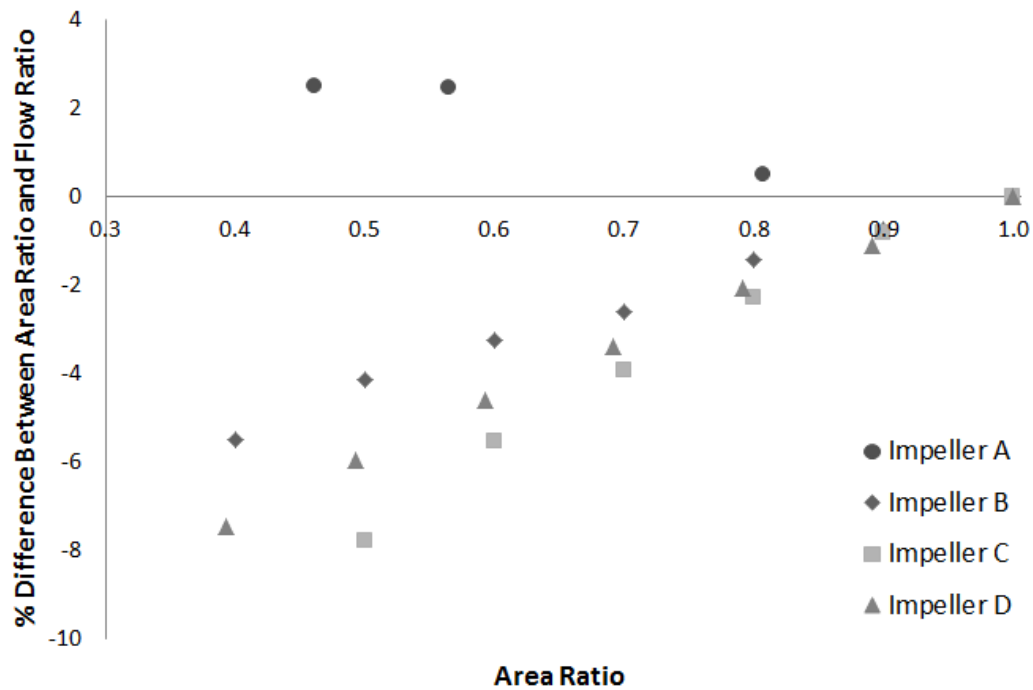


Figure 4.24: Percent Difference Between Flow Ratio and Area Ratio for Flow Trimmed Impellers

Chapter 5

Axial Trimming

5.1 Axial Trimming Methodology

For the axially-trimmed impellers, the trimming methodology is simpler than for the flow-trimmed impellers. Because it is desirable to apply trimming to the impeller in such a way that will require the least amount of redesign or permit as much of the original equipment to be reused with a modified impeller, the shroud profile is maintained per the original design and shifted axially into the impeller so that the blade height at the outlet is reduced. When the impeller is trimmed, the clearance gap is maintained at the nominal value. This is in contrast to Schumann's study [6,28] wherein the tip gap is reduced in proportion to the exit blade height. In doing so, the effects of trimming should be separated from the effects of reducing the tip gap. The exit area of the impeller is reduced by the equation:

$$Area\ Ratio = \frac{A_{2,trimmed}}{A_{2,baseline}} = \frac{b_{2,trimmed}}{b_{1,trimmed}}$$

For each baseline impeller design, a series of trims were applied as described until the inlet area of each impeller was trimmed by at least 60%. Each impeller trim is abbreviated by a letter-number designator where "A" identifies it as an axial trim and the number which follows is the percent outlet area reduction, so an "A30" trim represents an axial trim where the exit blade height has been reduced by 30%.

5.2 Axial Trim Results

As with the flow trimmed impellers, the baseline geometry for each impeller was trimmed and each trim meshed. Then, a speedline was produced for each of the impeller trims from choked flow and the back pressure raised progressively to the point that the steady-state CFD model failed to converge.

Head coefficient is plotted against flow coefficient in Figures 5.1 through 5.4.

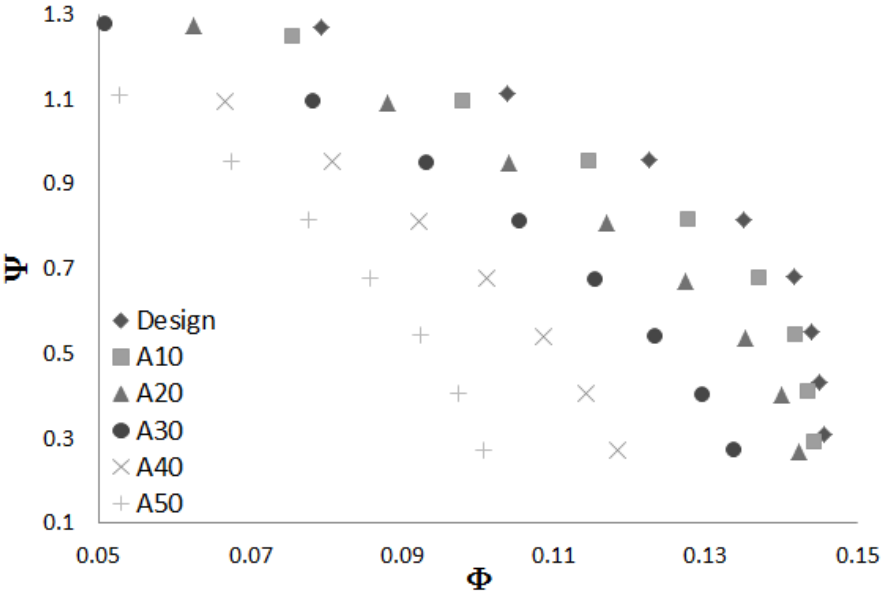


Figure 5.1: Head Coefficient vs. Flow Coefficient for Axially Trimmed Impeller A

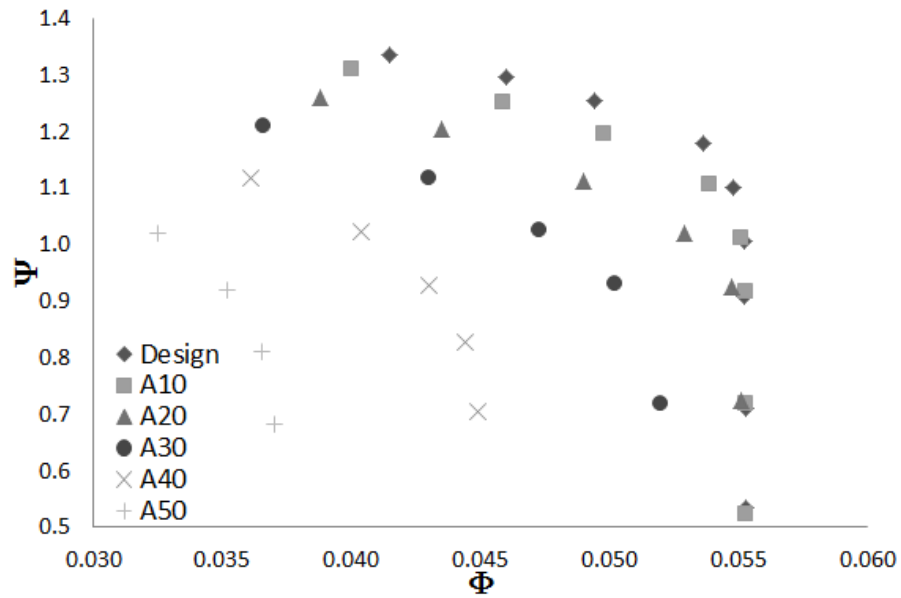


Figure 5.2: Head Coefficient vs. Flow Coefficient for Axially Trimmed Impeller B

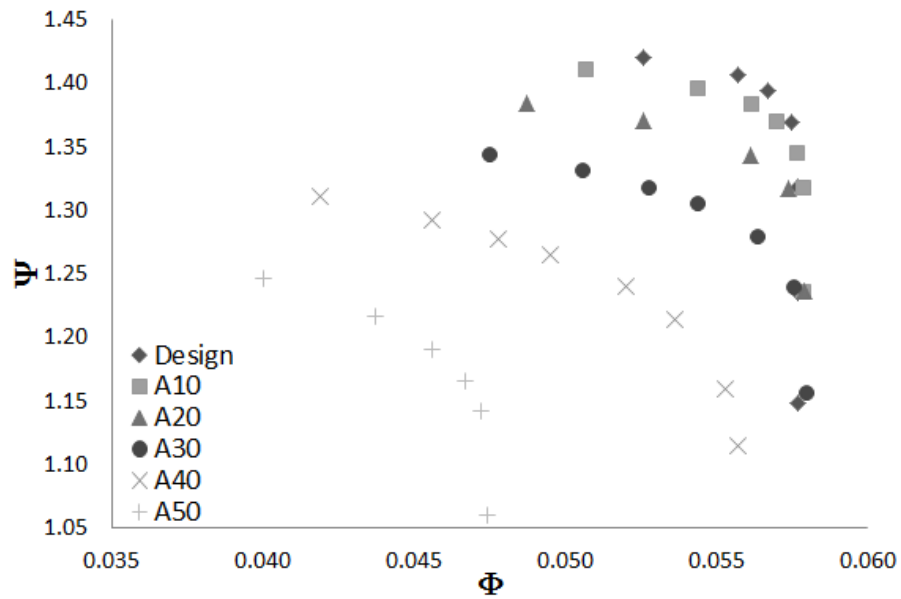


Figure 5.3: Head Coefficient vs. Flow Coefficient for Axially Trimmed Impeller C

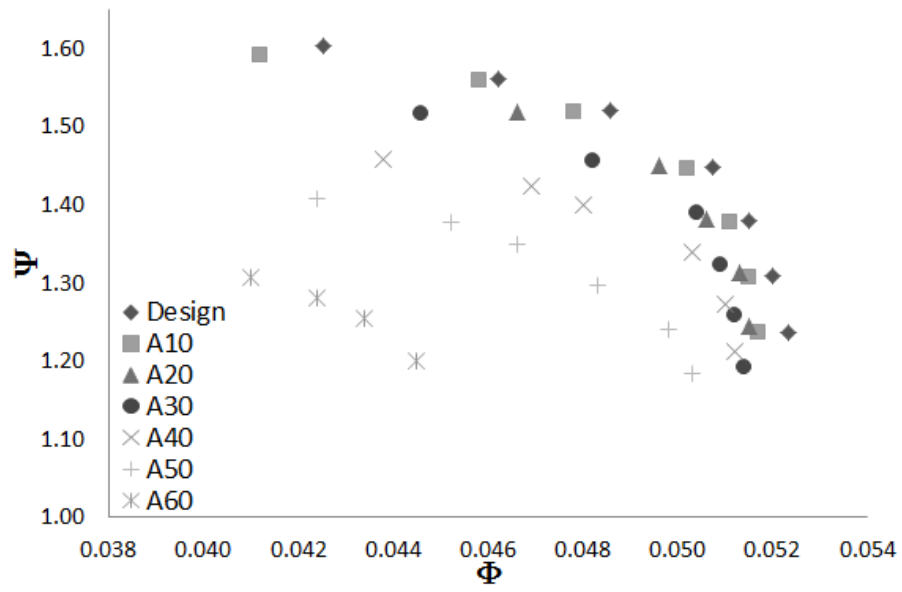


Figure 5.4: Head Coefficient vs. Flow Coefficient for Axially Trimmed Impeller D

These results show certain behaviors related to trimming for each of the impellers. Initially, as the impeller is trimmed, the head coefficient reduces, but the flow coefficient remains unchanged; in addition, the flow range of the impeller tends to increase. As was noted in Section 4.4, CFD has limited capability to predict the surge line of a compressor, but the consistency of the widening flow range is notable and may be predictive of real phenomena. As the impeller is trimmed further, the choked flow coefficient of each impeller is reduced. The point at which the choked flow coefficient reduces from the baseline value will be considered to be the limit of usefulness for axial trimming because the purpose is to reduce the pressure rise without reducing the flow range.

In terms of how trimming affects flow and pressure ratio, the head coefficient for Impeller A reduces with trimming, but the choked flow of the impeller begins to show reduction when it is trimmed 30%. Impeller B loses flow range when trimmed 40% and shows a more significant reduction in head coefficient than Impeller A. Impeller C can be trimmed up to 30% of the baseline exit blade height, and Impeller D tolerates trimming up to almost 40% before it loses flow range.

Another criterium for the beneficial use of axial trimming is efficiency. If trimming imposes a significant penalty to efficiency, then the usefulness is compromised and it may prove profitable to invest in a new impeller design. Plots of isentropic efficiency vs. flow coefficient for each of the four axially trimmed impellers are presented in Figures 5.5 through 5.8.

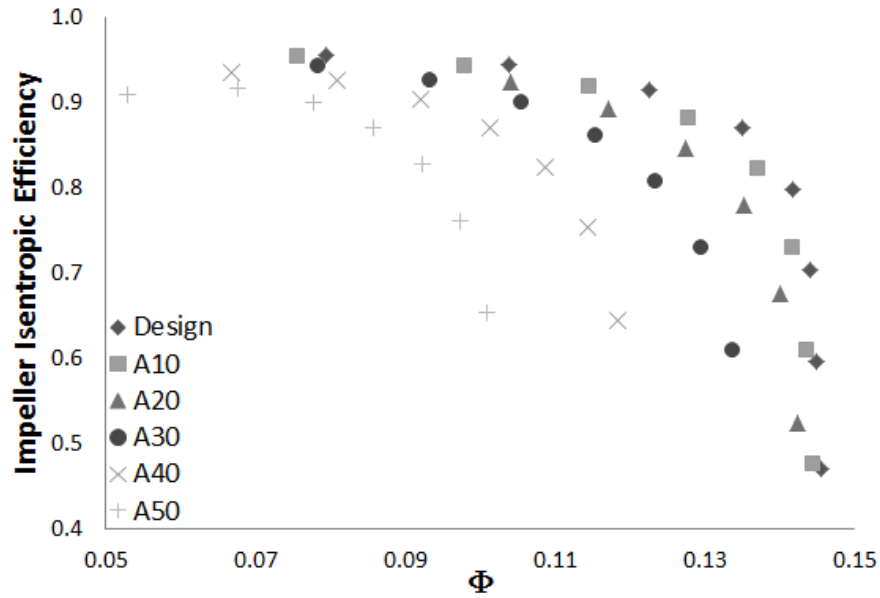


Figure 5.5: Total-to-Total Isentropic Efficiency vs. Flow Coefficient for Axially Trimmed Impeller A

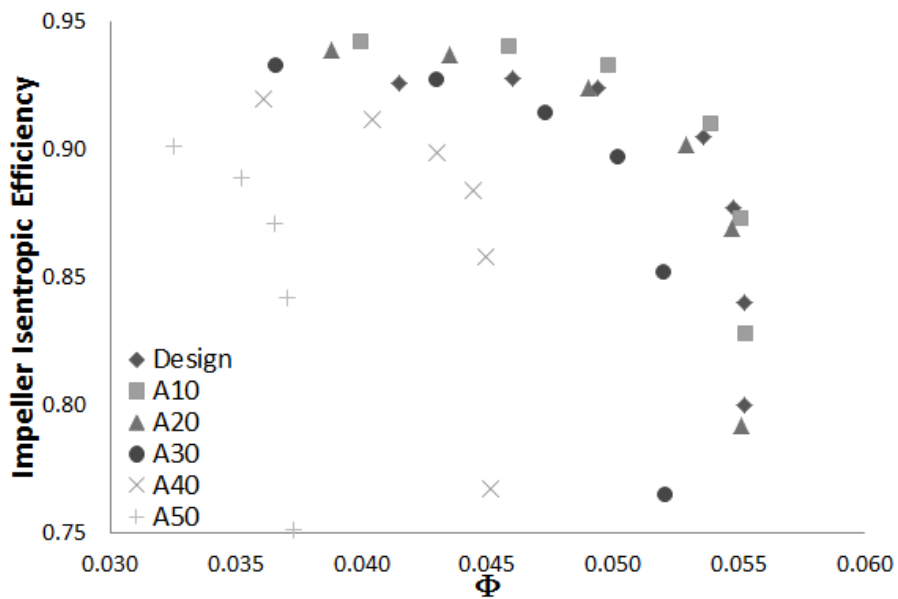


Figure 5.6: Total-to-Total Isentropic Efficiency vs. Flow Coefficient for Axially Trimmed Impeller B

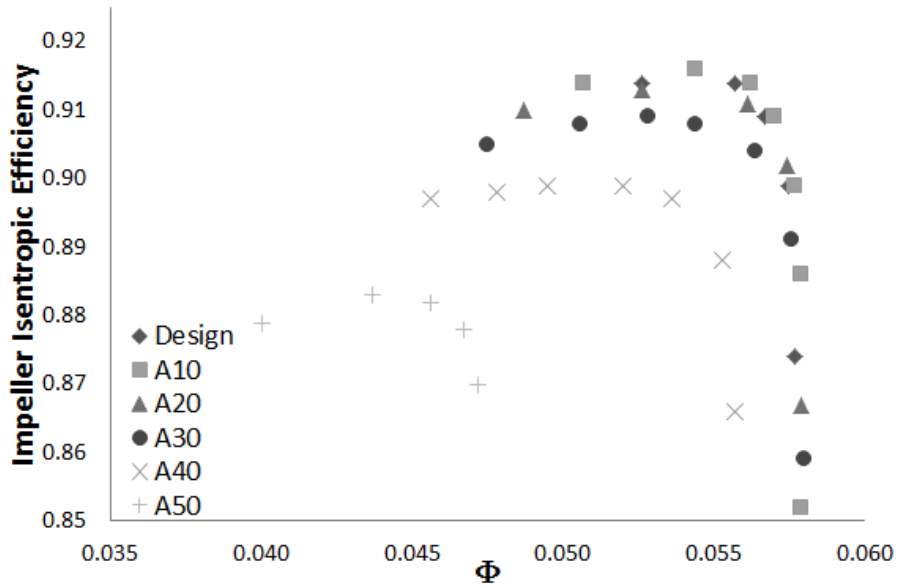


Figure 5.7: Total-to-Total Isentropic Efficiency vs. Flow Coefficient for Axially Trimmed Impeller C

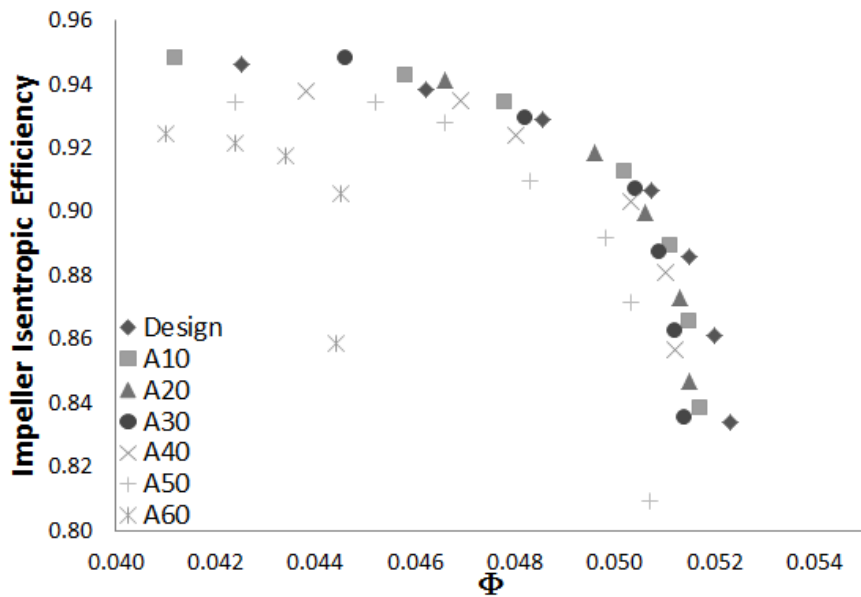


Figure 5.8: Total-to-Total Isentropic Efficiency vs. Flow Coefficient for Axially Trimmed Impeller D

Figure 5.8 shows efficiency performance near the baseline rate across the entire flow range of Impeller D up through the outlet blade height trimmed by 40% and only loses efficiency when the impeller is trimmed to the point that it can not achieve the baseline flow. Impeller C, while it maintains its flow range through a 30% outlet trim, suffers a significant efficiency penalty beginning at a 30% axial trim. Impeller B can only tolerate a small amount of trimming, but demonstrates impeller efficiency equal to or better than the baseline impeller when 10-20% of the outlet blade height is trimmed; and, although Impeller A exhibits a similar reduction in pressure ratio with trimming to Impeller B, according to Figure 5.5, it suffers a penalty to performance when axially trimmed as little as 20%.

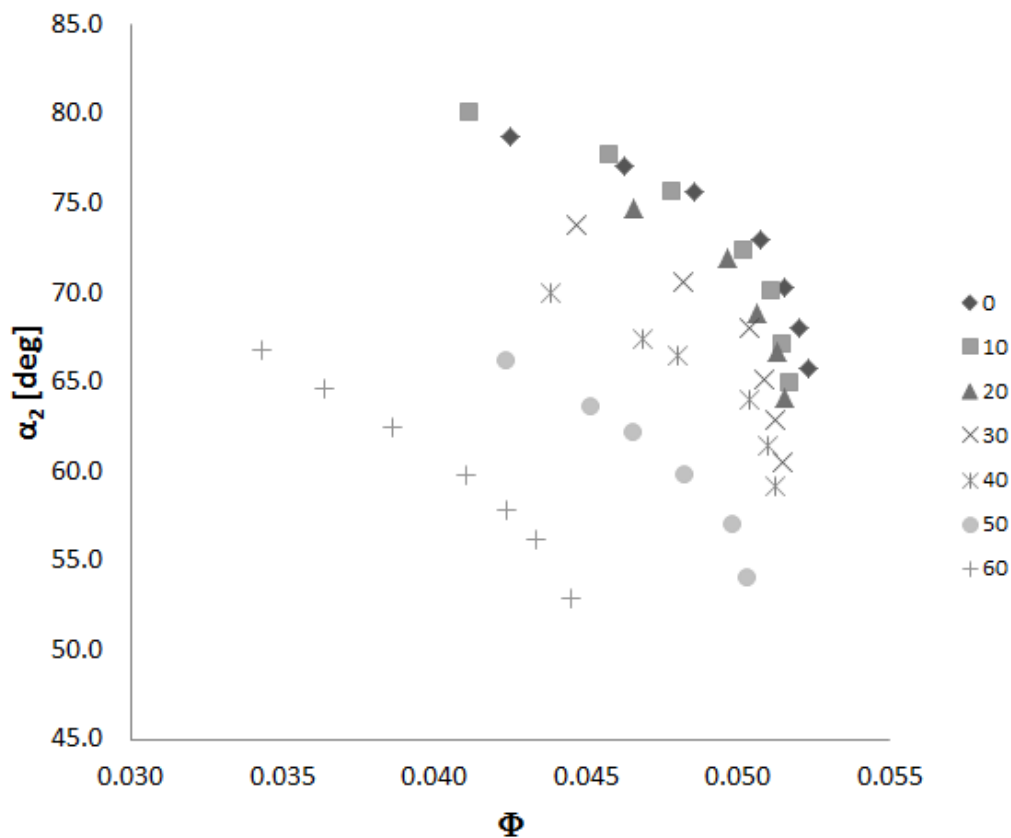


Figure 5.9: Exit Flow angle vs. Flow Coefficient for Axially-Trimmed Impeller D

The mass-averaged exit flow angle (α_2) is plotted against flow coefficient for Impeller D

in Figure 5.9. This plot shows a reduction in exit flow angle for the same flow coefficient as the impeller is trimmed. This is an important parameter for outlet trimming because the mechanism by which axial trimming reduces the head coefficient of an impeller is by reducing the area in the radial portion of the passage causing a higher throughflow velocity and reducing the amount of diffusion in the passage. The result is a more radial flow angle at the exit. This relationship between exit flow angle and pressure rise can be seen in one-dimensional analysis where; given the same gas properties, inlet and exit blade angles, rotational speed, and efficiency; pressure ratio becomes a function of exit flow angle. [1]

$$\frac{P_{o2}}{P_{o1}} = \left[1 + \frac{(\gamma - 1)\eta U_2^2 \tan\alpha_2}{a_{o1}^2 (\tan\alpha_2 + \tan\beta_2)} \right]^{\frac{\gamma}{\gamma-1}}$$

As the throughflow velocity increases with axial trimming, there comes a point at which the flow in the passage reaches sonic velocity and the choke point of the impeller moves from the inlet to the radial portion of the passage. This is what causes the flow range to reduce as the impeller is trimmed. This behavior is demonstrated in Figure 5.10 which shows a plot of the relative mach number in the impeller passage at the mid-span near the impeller exit. The operating point for each of these is near-choke, so the baseline case shows Mach numbers well below sonic velocity because the choke point is at the inlet. The A30 (30% axially-trimmed) case shows increasing velocity due to trimming at the outlet, and the A60 case demonstrates the choke point moving to a point near the exit of the passage.

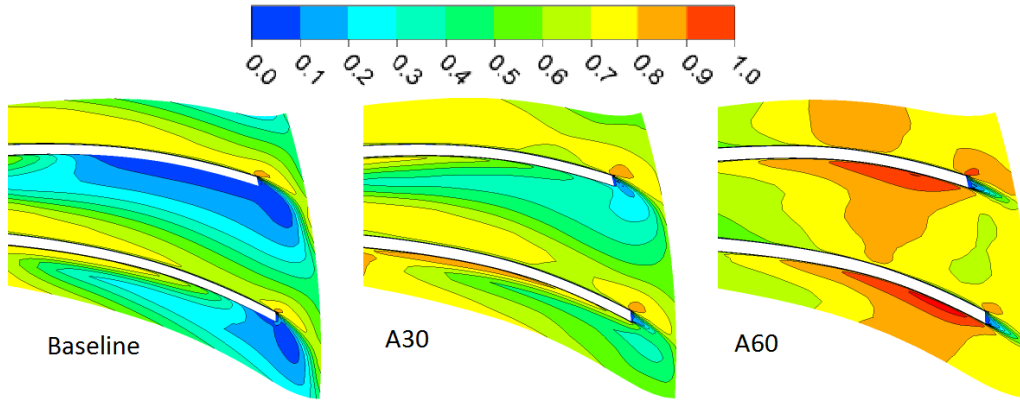


Figure 5.10: Relative Mach Number at Impeller Exit Near Choke for Axially-Trimmed Impeller D at 50% Span

5.3 Analysis

According to the CFD study, the pressure ratio of a centrifugal impeller may be reduced without reducing the flow range by reducing the outlet height. This ability is limited in each case by choking in the impeller passage when the impeller is trimmed beyond a certain point, but that point varies based on the original design of the impeller. The impeller efficiency may or may not be maintained as the impeller is trimmed.

In his study, Schumann [6,28] performed an axial trim on a centrifugal impeller, and found a peak efficiency as the impeller was trimmed. The current study did not find trimming to have any benefit to efficiency; to the contrary, this study has found a potential penalty to efficiency with axial trimming. However, as discussed previously, Schumann varied the clearance gap as a function of exit blade height to maintain a constant ratio of tip clearance to b_2 while the current study uses a constant tip gap. Because of this, the two studies cannot be directly related; but the findings can be combined to conclude that efficiency gains found by Schumann can be attributed to the reduction in clearance alone and not to reduction in exit blade height.

According to Figures 5.1 through 5.4; in the un-choked region, to the left of the "knee" in the speedline curve, the lines of Ψ vs Φ are roughly parallel for the baseline and axially-trimmed impellers. The practical use of axial trimming is limited to those impellers which can operate in the same flow range as the baseline impeller; therefore, considering only those which do not choke in the passage, the reduction in head coefficient is plotted against the reduction of outlet height in Figure 5.11. In that figure, the $\Psi/\Psi_{baseline}$ is taken at the approximate center of the unchoked portion of the speedline. In each case, employing axial trimming allowed the head coefficient to be reduced by between 7 and 11 percent before choking in the passage limited the flow range. There was wide variance observed in the effect of outlet trimming on head coefficient; the outlet of Impeller D was trimmed up to 40% and produced a 9% reduction in pressure ratio, while Impellers A and B realized an 11% reduction in pressure ratio with an outlet height reduction of only 20%. According to Figure 5.11, the four impellers divide themselves clearly into two groups - Impellers A and B exhibit a much sharper decline in pressure ratio for a smaller reduction in outlet height while Impellers C and D may be trimmed to a greater degree while maintaining their flow range, but to lesser effect.

Referring back to the baseline performance characteristics presented in Table 4.2, it can be seen that impellers C and D have both lower specific speeds and higher diffusion ratios than impellers A and B. Impellers A and B have diffusion ratios not much greater than one, so most of the pressure rise comes from the centrifugal effect and produces only a small amount of static pressure rise in the impeller passage. Impellers C and D achieve a much higher ratio of static-to-total pressure rise in the impeller and this difference is reflected in how the impellers react to axial trimming. As an alternative to radial trimming, the results for axial trimming are promising, but inconclusive. There was not a strong correlation between high

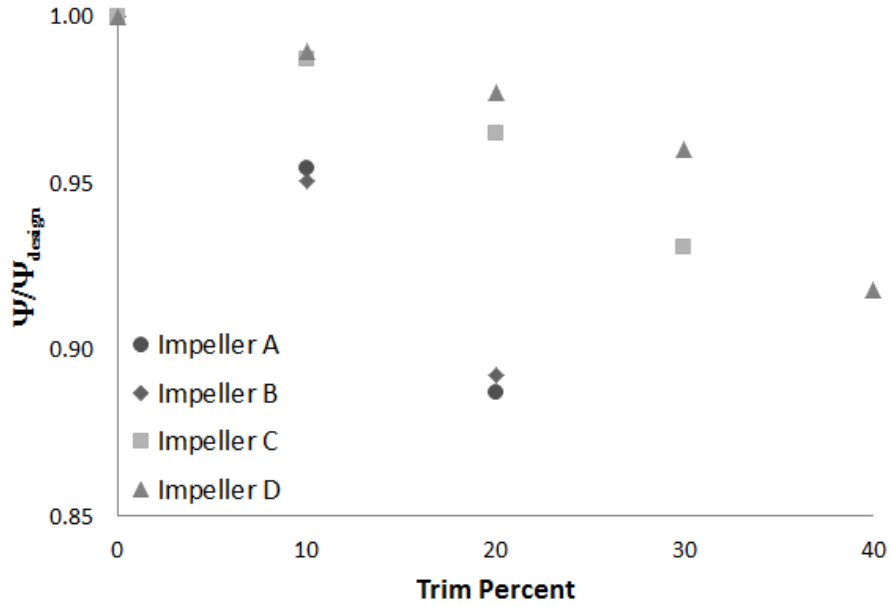


Figure 5.11: Ratio of Head Coefficient to Design Head Coefficient vs. Trim Percent

specific speed and tolerance for axial trimming. The pressure ratio of the higher specific speed impellers (A and B) were able to be reduced by axial trimming more than the low specific speed wheels; however, Impeller A suffered a significant efficiency penalty with trimming while Impeller B was particularly tolerant. This difference may be due to the shroud or the simple blading of Impeller A vs the more modern design of Impeller B.

Chapter 6

Conclusions

6.1 Summary

In this work, two types of centrifugal impeller blade trimming were studied using computational fluid dynamics. In the first type, flow trimming, the passage area is trimmed from inlet to exit. The purpose of flow trimming is to reduce the flow of the compressor while maintaining the pressure ratio. The second type of trimming, axial trimming, shifts the shroud line axially so that the exit blade height of the impeller without affecting the inlet geometry with the intent of reducing the pressure ratio of the compressor without changing the flow range.

Four impellers of widely differing geometric and performance parameters were selected for study. The geometry of each impeller was modeled using ANSYS BladeGen and a series of flow and axial trims were applied to each of the four impellers and each series of impellers was then meshed using ANSYS TurboGrid. Finally, the performance was modeled using ANSYS CFX and a speed line was created at the design speed for each series of trims by varying the back pressure and running a series of steady state performance points between choke and surge.

6.1.1 Flow Trimming

For the flow trimmed impellers, the results show that any of the four impellers may be trimmed to some extent while maintaining both pressure ratio and efficiency. The flow range decreased with trimming, but when the flow coefficient of each trim was normalized by the choked flow coefficient, it was seen that the relative flow range (that is, the surge margin) actually increased with flow trimming.

The choked flow coefficient of a trimmed impeller would be expected to scale in proportion with the inlet area of the impeller, but the results showed the choked flow coefficient to scale somewhat differently from the inlet area. The difference between the area ratio and the flow coefficient ratio was found to increase linearly with trimming in each case, and could be a positive or negative difference based on the baseline impeller design.

Different impeller baseline designs demonstrated different tolerances for flow trimming. Two of the impellers could be trimmed significantly (up to about 50% of the original area) without adversely affecting impeller efficiency or pressure ratio. The others suffered significant penalties to efficiency as the impeller was trimmed. An impeller's tolerance for flow trimming correlated with the flow incidence on the impeller wherein a positive incidence correlated with poor tolerance for flow trimming and a neutral or slightly negative incidence correlated with good tolerance for flow trimming.

6.1.2 Axial Trimming

In the case of the axially trimmed impellers, each of the impellers modeled were able to be trimmed so that the pressure ratio was reduced without adversely affecting the flow range or impeller efficiency. The mechanism by which the pressure ratio is reduced is reduced

diffusion in the passage leading to higher throughflow velocity and a more radial exit flow angle (α_2). In every case, the axial trimming was limited at some point by reduction of the choked flow rate. This reduction in choked flow was due to the fact that reducing the passage area in the radial portion of the passage moved the choke point from the inlet to the passage.

The performance impact of axial trimming varied significantly depending on the baseline design. Two of the impellers were able to have the head coefficient reduced by about 10% with about a 20% reduction in outlet height. The other impellers could be trimmed by at least 30% of the baseline outlet height, but the reduction in head coefficient was much less. The different behaviors correlated with diffusion ratio. The two impellers with baseline diffusion ratios around 1.2 were able to be trimmed little but to great effect. The other two impellers had baseline diffusion ratios of about 1.5 and 1.9 respectively and were able to be trimmed to a progressively greater degree but with progressively lesser effect.

6.2 Applicability to Design

Centrifugal impellers are simple machines with complex geometry. As such, they require significant design effort to produce a new aerodynamic design. If a successful existing design can be modified to produce a new impeller, then a large portion of the design effort may be bypassed. Traditionally, this has been accomplished by applying the laws of similitude to existing designs. The application of impeller blade trimming adds more arrows to the quiver of design strategies, but they must be applied with careful consideration.

If an impeller is flow trimmed, then peripheral components such as the shroud and diffuser must also be redesigned. The application of an axial trim has the advantage of maintaining

the same shroud profile, but the diffuser still requires redesign due to the reduced exit blade height and change in exit flow angle for an axially trimmed impeller.

While some of the impellers investigated demonstrated high tolerance for flow and/or axial trimming, others did not and so careful consideration should be given to whether the baseline design is appropriate for trimming. Based on the results of this and other trimming studies, a safe course of action would be to limit the application of trimming to small changes of flow or pressure ratio, because each of the impellers studied were able to be both flow trimmed or axial trimmed small amounts without significant loss of efficiency. Larger changes may be possible, but the designer must consider whether the baseline impeller is appropriate to be trimmed.

6.3 Next Steps

This study represents a significant step forward in the understanding of the effects of centrifugal impeller blade trimming because, whereas previous studies examined the effects of trimming on a single design, this work compared trimming effects for four different impeller designs. However, there are still questions that remain unanswered and the results raise additional questions. While a sample set of four impellers is a significant improvement from previous works, it still represents a small sample. Expanding the work to include additional designs would help to confirm or refine the conclusions of this study. Of the four impeller designs, only one was shrouded. It was this shrouded impeller that exhibited a different trend of area ratio to flow ratio from the other three, and it's not clear if that has to do with the fact that it was a shrouded design or if it was due to other aspects of the design. The question as to whether high specific speed designs are particularly well-suited to axial

trimming remains open, and there is a new question about whether shrouded compressor designs are particularly intolerant of axial trimming. This work provides a broader overview of the application of centrifugal impeller blade trimming than has previously been available, but the topic still holds fruitful areas for new research.

BIBLIOGRAPHY

BIBLIOGRAPHY

- [1] Dixon, S. L., 2005. *Fluid Mechanics and Thermodynamics of Turbomachinery*. Elsevier Butterworth-Heinemann.
- [2] Krain, H., 2003. “Review of centrifugal compressor’s application and development”. In Proceedings of ASME Turbo Expo.
- [3] Boyce, M. P., 2012. *Gas Turbine Engineering Handbook (Fourth Edition)*. Butterworth-Heinemann.
- [4] Cordier, O., 1955. “Similarity considerations in turbomachines”. *VDI Report*, **3**, p. 85.
- [5] Japikse, D., 1996. *Centrifugal Compressor Design and Performance*. Concepts ETI, Inc., Wilder, VT.
- [6] Schumann, L. F., Clark, D. A., and Wood, J., 1987. “Effect of area ratio on the performance of a 5.5:1 pressure ratio centrifugal impeller”. *Journal of Turbomachinery*, **109**, pp. 10–19.
- [7] Senoo, Y., and Ishida, M., 1987. “Deterioration of compressor performance due to tip clearance of centrifugal compressors”. *Journal of Turbomachinery*, **109**, pp. 55–61.
- [8] Lüdtke, K. H., 2004. *Process Centrifugal Compressors*. Springer-Verlag.
- [9] Stodola, A., 1945. *Steam and Gas Turbines. Vols. I and II*. McGraw-Hill.
- [10] Dean, R. C., and Senoo, Y., 1960. “Rotating wakes in vaneless diffusers”. *Trans ASME Journal of Basic Engineering*, **82**, pp. 563–574.
- [11] Cumpsty, N., 1989. *Compressor Aerodynamics*. Krieger Publishing Company.
- [12] Rodgers, C., 1964. “Typical performance characteristics of gas turbine radial compressors”. *Journal of Engineering for Power*, **86**, pp. 161–175.
- [13] Harada, H., 1988. “Performance characteristics of two- and three-dimensional impellers in centrifugal compressors”. *Journal of Turbomachinery*, **110**, pp. 110–114.

- [14] Bonaiuti, D., and Zangeneh, M., 2009. “On the coupling of inverse design and optimization techniques for the multiobjective, multipoint design of turbomachinery blades”. *Journal of Turbomachinery*, **131**, pp. 021014–1 – 021014–16.
- [15] Ibaraki, S., Matsuo, T., Kuma, H., Sumida, K., and Suita, T., 2003. “Aerodynamics of a transonic centrifugal compressor impeller”. *Journal of Turbomachinery*, **125**, pp. 346–351.
- [16] Ibaraki, S., Sumida, K., and Suita, T., 2009. “Design and off-design flow fields of a transonic centrifugal compressor impeller”. In Proceedings of ASME Turbo Expo 2009: Power for Land, Sea and Air, no. GT2009-59986.
- [17] Schleer, M., Song, S. J., and Abhari, R. S., 2008. “Clearance effects on the onset of instability in a centrifugal compressor”. *Journal of Turbomachinery*, **130**, pp. 031002–1 – 031002–11.
- [18] Harada, H., 1985. “Performance characteristics of shrouded and unshrouded impellers of a centrifugal compressor”. *Journal of Engineering for Gas Turbines and Power*, **107**, pp. 528–533.
- [19] Al-Zubaidy, S. J. J., 1992. “Axial length influence on the performance of centrifugal impellers”. *Journal of Propulsion and Power*, **8**, pp. 1245–1251.
- [20] Aungier, R. H., 2000. *Centrifugal Compressors: A Strategy for Aerodynamic Design and Analysis*. American Society of Mechanical Engineers.
- [21] Sorokes, J. M., Kopko, J. A., Geise, P. R., and Hinklein, A. L., 2009. “The influence of shroud curvature and other related factors on impeller performance characteristics”. In Proceedings of ASME Turbo Expo 2009: Power for Land, Sea and Air, no. GT2009-60109.
- [22] Godse, A. G., 1989. Predict compressor performance at new conditions. Hydrocarbon Processing, June.
- [23] Liu, C., Tan, J., Qi, D., Wang, X., and Qin, G., 2011. “A practical approximate method to predict adjusting performance of a centrifugal compressor stage with inlet guide vane”. In Proceedings of ASME Turbo Expo 2011, no. GT2011-45195.
- [24] Rodgers, C., 2001. “Centrifugal compressor blade trimming for a range of flows”. In Proceedings of ASME Turbo Expo.

- [25] Zhang, D., DiLiberti, J.-L., and Cave, M., 2010. “A cfd study on a base and a flow-trimmed low specific speed centrifugal compressor”. In Proceedings of the ASME 2010 International Mechanical Engineering Congress & Exposition, no. IMECE2010-40561.
- [26] Sapiro, L., 1983. “Effect of impeller-extended shrouds on centrifugal compressor performance as a function of specific speed”. *Journal of Engineering for Power*, **105**, pp. 457–465.
- [27] Engeda, A., 2007. “Effect of impeller exit width trimming on compressor performance”. In 8th International Symposium on Experimental and Computational Aerothermodynamics of Internal Flows, no. ISAIF8–00135, Ecole Centrale de Lyon.
- [28] Schumann, L. F., Clark, D. A., and Wood, J. R., 1986. “Effect of area ratio on the performance of a 5.5:1 pressure ratio impeller”. In Proceedings of the International Gas Turbine Conference and Exhibit, no. 86-GT-303.
- [29] Nili-Ahmadabadi, M., Hajilouy-Benisi, A., Durali, M., and Motavalli, S. M., 2008. “Experimental and numerical investigation of a centrifugal compressor and numerical study of the area ratio and tip clearance effects on the performance characteristic”. In Proceedings of ASME Turbo Expo 2008: Power for Land, Sea and Air, no. GT2008-50969.
- [30] David, T., Zhang, D., and Cave, M., 2006. “Frictional effects on a base and a flow-trimmed impeller of a low specific speed industrial compressor”. In Proceedings of ASME Turbo Expo.
- [31] Ansys cfx [computer software]. version 13.0. canonsburg, pa: Ansys, inc.; 2010.
- [32] Zikanov, O., 2010. *Essential Computational Fluid Dynamics*. John Wiley & Sons.
- [33] Ferziger, J., and Perić, M., 1996. *Computational Methods for Fluid Dynamics*. Springer-Verlag.
- [34] Spalart, P. R., and Allmaras, S. R., 1994. “A one equation turbulence model for aerodynamic flows”. *Recherche Aerospaciale*, **1**, pp. 5–21.
- [35] Bladegen [computer software]. version 13.0. canonsburg, pa: Ansys, inc.; 2008.
- [36] Turbogrid [computer software]. version 13.0. canonsburg, pa: Ansys, inc.; 2010.
- [37] McKain, T. F., and Holbrook, G. J., 1997. Coordinates for a high performance 4:1 pressure ratio centrifugal compressor. Tech. Rep. NASA CR-204134, NASA.

- [38] Osborne, C., Runstadler-Jr., P., and Stacy, W. D., 1975. Aerodynamic and mechanical design of an 8:1 pressure ratio centrifugal compressor. Tech. Rep. NASA CR-134782, NASA.
- [39] Pampreen, R. C., 1977. Splitter-bladed centrifugal compressor impeller designed for automotive gas turbine application. Tech. Rep. NASA-CB-135237, NASA.
- [40] Vagani, M., 2013. “Prediction of impeller rotating stall onset using numerical simulations of a centrifugal compressor. part 1: Detection of rotating stall using fixed-flow transient simulations”. *Proc. IMechE Part A: J. Power and Energy*, **227**, pp. 403–414.
- [41] Cornelius, C., Biesinger, T., Galpin, P., and Braune, A., 2014. “Experimental and computational analysis of a multistage axial compressor including stall prediction by steady and transient cfd methods”. *Journal of Turbomachinery*, **136**, pp. 061013–1 – 061013–12.